MAGMA DIFFERENTIATION AT NEWBERRY CRATER IN CENTRAL OREGON

by

ROBERT LEE BEYER

A DISSERTATION

Presented to the Department of Chemistry
and the Graduate School of the University of Oregon
in partial fulfillment
of the requirements for the degree of
Doctor of Philosophy

December 1973

ACKNOWLEDGEMENTS

The writer wishes to express his thanks to Dr. G. G. Goles for his assistance and encouragement rendered during this investigation. I also wish to thank D. B. Stoeser, L. F. Henage, and J. W. Stoeser for their advice and suggestions given throughout this study, D. J. Lindstrom for his part in collecting samples, and W. P. Leeman for kindly providing splits of his Lava Butte samples.

This research was supported by NSF research grants GA-19382 and GA-33154.

PUBLICATIONS:

Instrumental neutron activation analysis of lunar specimens (with G. G. Goles, M. Osawa, K. Randle, D. Y. Jerome, D. J. Lindstrom, M. R. Martin, S. M. McKay, and T. L. Steinborn); Science 167, 497-499 (1970).

Interpretations and speculations on elemental abundances in lunar samples (with G. G. Goles, K. Randle, M. Osawa, D. J. Lindstrom, D. Y. Jerome, T. L. Steinborn, M. R. Martin, and S. M. McKay; Proc. Apollo 11 Lunar Science Conference, Geochim. Cosmochim. Acta, Supplement I, 2, 1177-1194 (1970).

Analysis of Apollo 12 specimens: compositional variations, differentiation processes, and lunar soil mixing models (with G. G. Goles, A. R. Duncan, D. J. Lindstrom, M. R. Martin, M. Osawa, K. Randle, L. T. Meek, T. L. Steinborn, and S. M. McKay); Proc. of the Second Lunar Science Conference 2, 1063-1081, The M. I. T. Press (1971).

TABLE OF CONTENTS

	Page
ACKNOWLEDGEMENTS	iii
VITA	iv
TABLE OF CONTENTS	vi
LIST OF TABLES	viii
LIST OF FIGURES	ix
INTRODUCTION	1
NEWBERRY CALDERA - DESCRIPTION AND GEOLOGY	3
Regional Setting	3
Physiography	6
Structure	7
Volcanic Sequence	9
Previous Investigations	10
DATA AND RESULTS	12
Analytical	12
Sample Notes	25
Observations	29
DIFFERENTIATION OF MAGMAS	33
IMPLIED MAGMA DIFFERENTIATION PROCESSES AT NEWBERRY CRATER	38
Mixing	38
Volatile Transfer	39
Fractional Crystallization	40
SOME ASPECTS OF PARTIAL MELTING	64
SUMMARY AND CONCLUSIONS	68
BIBLIOGRAPHY	70

Page

APPENDIX I: SAMPLE LOCATIONS 74

Basalt-Andesites 74
High-Iron Basalts 76
Amota Butte Series 76
Rhyolites 76
Newberry Area Samples 77

APPENDIX II: MOLECULAR NORM CALCULATIONS 82

LIST OF TABLES

Table		Page
1a	Chemical Analyses and Molecular Norms	14
1b	Chemical Analyses and Molecular Norms	15
1c	Chemical Analyses and Molecular Norms	16
1d	Chemical Analyses and Molecular Norms	17
1e	Chemical Analyses and Molecular Norms	18
1f	Chemical Analyses and Molecular Norms	19
2	Selected Partition Coefficients from the Literature	42
3	Compositions of Minerals Used in Mixing Models	50
4	Analyses and Averages Used in Mixing Models	52
5	Results of Mixing Model Processes	55
6a	Trace Element Results Using Crystal Fractionation Processes	59
6b	Trace Element Results Using Crystal Fractionation Processes	60
6c	Trace Element Results Using Crystal Fractionation Processes	61

LIST OF FIGURES

Figure		Page
1	Geological Map of Newberry Volcanic Area	4
2	Geological Sketch Map of Newberry Crater	8
3a	Variation Diagrams of Chemical Analyses	20
3b	Variation Diagrams of Chemical Analyses	21
3c	Variation Diagrams of Chemical Analyses	22
3d	Variation Diagrams of Chemical Analyses	23
4	Comparison of Iron Values Obtained by XRF and INAA	24
5	Frequency Distributions for SiO_2, Na_2O, and FeO	30
6	Rare Earth Element Plots for a Basalt and a Rhyolite from the Newberry Suite	32
7	The Diopside-Fosterite-Silica System	66
I-1a	Newberry Crater Quadrangle NW 1/4 (1935)	78
I-1b	Newberry Crater Quadrangle NE 1/4 (1935)	79
I-1c	Newberry Crater Quadrangle SW 1/4 (1935)	80
I-1d	Newberry Crater Quadrangle SE 1/4 (1935)	81

INTRODUCTION

Seismic evidence indicates that the crust of the Earth varies in thickness from about five kilometers in the oceans to an average of about thirty-five kilometers under the continents. Continental crust in general has an upper zone of granitic composition, and a lower zone believed to be of gabbroic composition. The crust has a slightly lower overall density than the material of the upper mantle which lies directly below it and is believed to rest in isostatic equilibrium on that material.

The upper mantle has a thickness of approximately four hundred kilometers. Little can be said about its exact chemical composition or mineral composition except where seismic evidence can be compared to various kinds of experimental evidence. It is believed that many magmas are formed as a result of processes occurring within the upper mantle. These magmas must then pass through part of the upper mantle and the crust to form igneous rocks observed on the Earth's surface.

Many observable extrusive rocks can be usefully classified in terms of their silica contents and a large range of silica contents is found in various igneous rocks. There is no reason to believe that each rock type was created separately at depth and then transported directly to the

Earth's surface unaltered. Rather, it is likely that in many cases observed suites of igneous rocks are linked to some parental magma or limited number of parental magmas. However, one cannot claim that magmas formed in the upper mantle are exactly uniform from place to place and with the passing of time, so that the characteristics of parental magmas are not well determined.

In this commonly accepted view, some process must occur to a magma, either when it is formed or some time between its formation and its emplacement and cooling, that would account for the differences one sees in suites of igneous rocks at the surface of the Earth. The process of changing the composition of a magma so as to produce different types of observable rocks is called differentiation. In some situations, basalts (average SiO_2 = 48%) and rhyolites (average SiO_2 = 72%) occur together in time and space without intermediate rocks to represent a continuous range of silica content. These occurrences have been termed basalt-rhyolite associations. It has been frequently hypothesized that a magma of basaltic composition was differentiated to an extreme composition by some mechanism to form rhyolitic rocks.

It is the purpose of this dissertation to present analytical data concerning rocks found at Newberry Crater in Central Oregon, a classic basalt-rhyolite association, and to use those data to examine some processes of magma differentiation.

NEWBERRY CALDERA - DESCRIPTION AND GEOLOGY

Regional Setting

Newberry Caldera (crater in common usage) is located near the top of a Pleistocene shield volcano about 35 miles east of the crest of the High Cascade range and about 25 miles south of Bend in Central Oregon, as shown in Figure 1. It lies near three volcanic provinces: 1) the Columbia Plateau to the northeast; 2) the Cascade province to the west; and 3) the Basin-and-Range province to the southeast. The boundaries of the Miocene provinces associated with each of these presently recognized provinces are generally poorly defined, but Newberry Volcano may lie near the junction of these provinces.

The Miocene Columbia lavas of Oregon and Washington mainly consist of tholeiitic basalts (Waters, 1961). Some of these lava flows are found about 40 miles to the northeast of Newberry Volcano in the Murray Mountains and are dipping in a southerly direction, but their extent south and west of the Murray Mountains is unknown.

The Miocene Cascade province of the Western Cascades consists of a series of eroded mountain ranges with a predominately northerly trend paralleling the High Cascades. They are composed of tuffs and lava flows and dip easterly

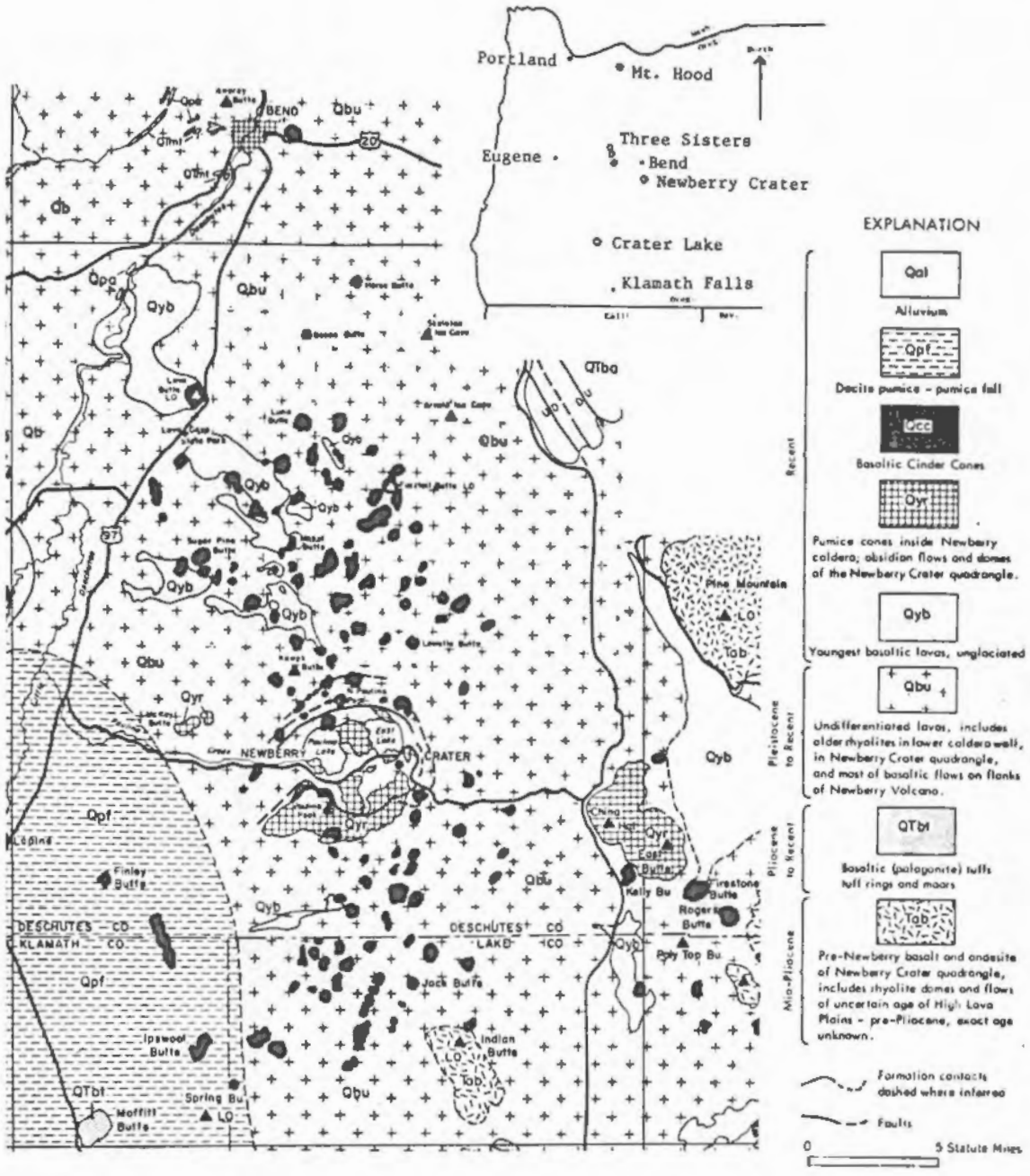

Figure 1. Geological Map of the Newberry Volcanic Area. Adapted from Peterson and Groh (1965) and Higgins (1973).

under the High Cascades. In the area west of Newberry Crater, their easterly extent is unknown, but further north they are exposed east of the High Cascades.

The northern part of the Basin-and-Range volcanic province ranges from late Miocene to Quarternary in age and is composed of high-alumina basalts with minor amounts of rhyolites and andesites. Their extent near Newberry Volcano is hidden by lake beds.

Newberry Volcano belongs to the Plio-Pleistocene High Cascade province with its well-known stratovolcanoes. These stratovolcanoes are composed mainly of hypersthene-andesites. The shields underlying them contain much high-alumina basalt. Recent cinder cones are relatively common and dacite and rhyodacite differentiates are found on many of the larger volcanoes.

Most of the plateau upon which Newberry Volcano lies is covered with pumice from Mount Mazama. To the north and east, much of the area is covered with basalt cap-rocks overlying the rocks of the John Day and Clarno formations, but these are not exposed close to Newberry Volcano. Further to the north in the Deschutes River valley, there is evidence to indicate that the river valleys were at one time filled with lavas from the nearby High Cascades. To the south and southeast lie lacustrine deposits of Pleistocene lakes mantled with pumice. Explosion craters and tuff rings are numerous. Lorenz (1970) studied a large explosion crater,

Hole-in-the-Ground, located about thirty miles south of Newberry Volcano and found diktytaxitic basaltic rock fragments of unknown origin which may correspond to early Newberry or High Cascade rocks. To the west lies the north-south trending Cascade Mountain range.

Physiography

The shield of Newberry Volcano has a basal diameter of approximately 20 miles and rises about 4000 feet above the surrounding plateau (Williams, 1935). The highest point, South Paulina Peak, rises 7,985 feet above sea level and forms part of the southwest section of the rim of Newberry Caldera.

The caldera is about 5 miles long and 4 miles wide and is bounded by cliffs up to 1500 feet high except on its west side, which has been down-faulted. The floor of the caldera contains two lakes, East Lake and Paulina Lake.

The slopes of the volcano are not deeply eroded at present and are now covered with recent pumice from Mount Mazama and, on the southeast, from Newberry itself. Hundreds of post-pumice cinder cones and several lava flows occur on the slopes of the volcano.

Although basaltic cinder cones and flows are the predominant features on the slopes of Newberry Volcano, rhyolite domes covered with Mazama pumice are also found east of the caldera (China Hat and East Buttes) and west of the

caldera (McKay Buttes). These domes along with the rhyolite domes and flows in Newberry Caldera and those further east form an east-west trend of rhyolitic volcanic activity. Figure 1 is a geological map showing the Newberry Crater area and Figure 2 is a geological map by Higgins (1973) showing various rock units and locations in the caldera.

Structure

Faults play a major role in the history of Newberry Volcano and are described by Higgins (1973). The volcano is located near the bend of the Brothers Fault Zone where it turns from a northwest-southeast trend, east of Newberry Volcano, to follow the Cascade range north of Newberry Volcano. Green Ridge, about 50 miles to the northwest, was formed by a major north-south fault. The Walker Rim, about 30 miles to the southwest, was formed by a fault which, if extended, would pass through Newberry Volcano. Further to the south, many north-south trending faults are found in the Basin-and-Range province. The closest "pre"-Newberry volcanic rocks are exposed in northwest-southeast trending faults on Pine Mountain, located about 12 miles east-northeast of the caldera, and at Indian Springs and Amota Buttes, located about 10 miles south of the caldera.

The west side of the caldera rim is down-faulted relative to the rest of the volcano, thereby providing for the natural drainage of the caldera rather than for another

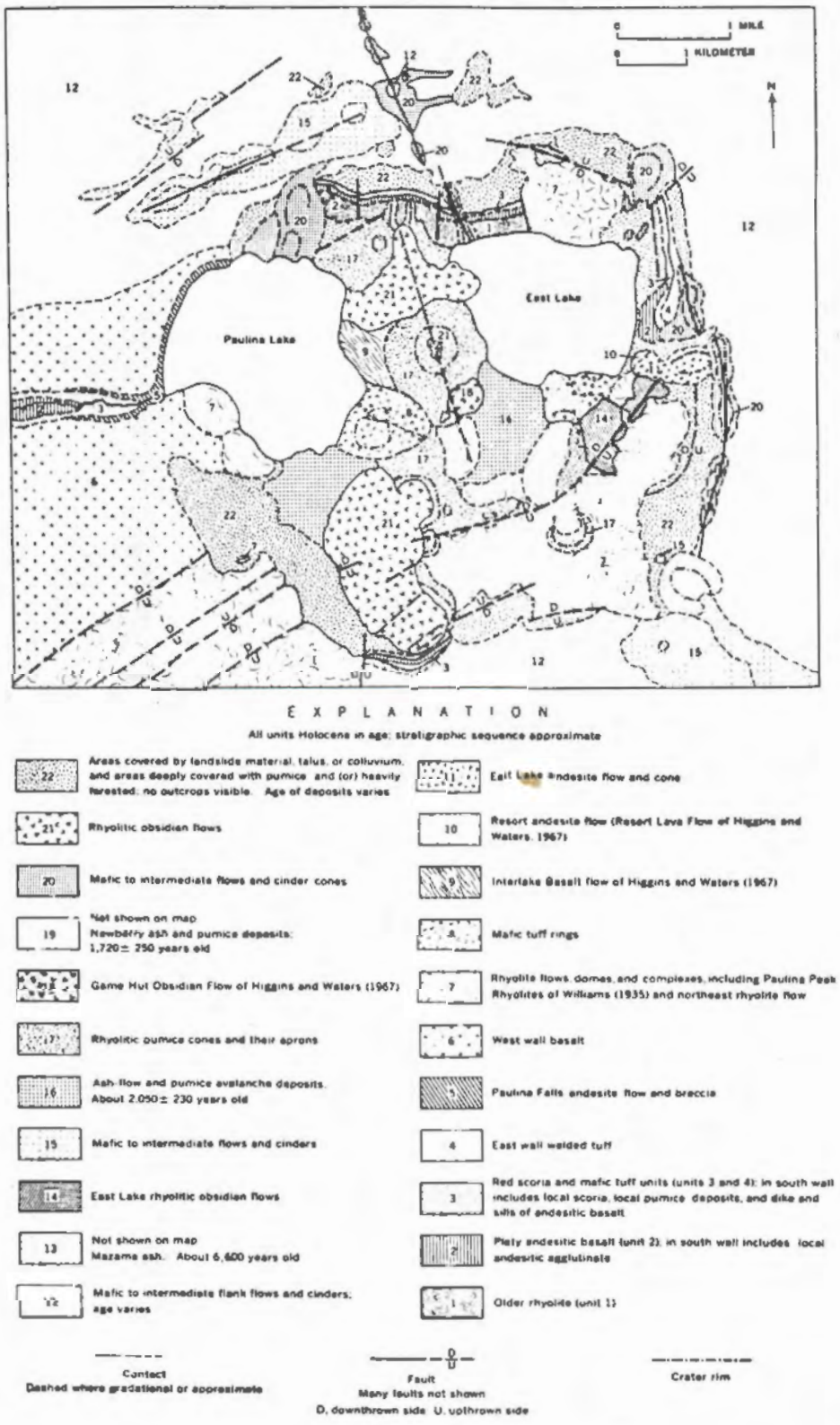

Figure 2. Geological Sketch Map of Newberry Crater (Higgins, 1973).

Crater Lake. Many of the cinder cones on the slopes are aligned on faults. Faults apparently form concentric rings related to the north and east rims and probably contributed to the collapse of the caldera. Some faults show trends radially away from the caldera, one of which extends from the caldera northwest to Lava Butte (on Highway 97) and along which are located the vents for several lava flows and cinder cones. On the northeast flank of the volcano, northwest-southeast lineations can be noted from the locations of cinder cones and are probably directly related to the Brothers Fault Zone.

Little can be definitely stated about the basement rocks under Newberry Volcano. Likewise, little can be said about the history of Newberry Volcano itself because the slopes are covered with a mantle of Mazama ash.

Volcanic Sequence

The oldest exposed rocks in the caldera are rhyolites which are found in the lower part of the caldera wall. Outside the caldera, the Amota Butte rocks, occurring about 10 miles southeast of the caldera, are probably the oldest exposed rocks but no time correlation between them and the caldera wall rocks is possible.

Higgins and Waters (1967) established a sequence of pre-collapse rocks on the basis of their occurrences in the

walls of the caldera. Their sequence includes the early rhyolites, andesites, scoria, and tuffs. Late in that sequence some lava flows and cinder cones were erupted on the flanks of the volcano. Mazama pumice, from the eruption which formed Crater Lake, covered the entire area about 7000 years B. P. (before the present time), thereby providing a convenient time marker in the area.

Cinder cones were erupted following the Mazama pumice. Newberry pumice, the Paulina Peak rhyolites, and the down-faulting of the west rim are associated with the formation of the caldera. The caldera was probably not formed in a single event, but is thought to have been formed by many smaller events over a period of years. The Newberry pumice, found inside the caldera and principally to the southeast, has been dated at 2054 ± 60 years B. P. (Libby, 1952) and 1270 ± 60 years B. P. (Peterson and Groh, 1969). The contrast in dates may indicate that more than one eruption of Newberry pumice occurred although field evidence supporting this hypothesis is lacking.

Cinder cones were erupted on the flanks of the volcano and both rhyolites and basalts have been erupted on the floor of the caldera since the Newberry pumice fall.

Previous Investigations

Newberry Crater first appears in recorded history when in 1826 it was visited by fur hunters. Early settlers knew

the area as the Paulinas because it was one of the hunting grounds for a Paiute raider, Chief Paulina. J. C. Russel first described Newberry mountain and its crater in 1905 and named it Newberry Volcano after John J. Newberry, a scientist who visited it in 1905 with the Williamson Railroad survey party. Williams (1935) described the geography, geology, history, and petrology of Newberry Volcano. Peterson and Groh (1965) and Higgins and Waters (1968) include field trip descriptions of Newberry Crater, and Higgins and Waters (1967) and Higgins (1973) describe the petrology of the rocks at Newberry Crater. Laidley and McKay (1971) showed the Big Obsidian Flow to be chemically highly homogeneous, in agreement with Osborn and Schmitt (1970) who studied manganese and sodium homogeneity in meteorites and used the Big Obsidian Flow as a standard. Peterson and Groh (1969) report ages of 1000 to 6000 B. P. for some flows and domes at Newberry Crater using methods of radio-carbon dating and obsidian hydration rind dating.

DATA AND RESULTS

Analytical

Samples from Newberry Crater were collected by D. J. Lindstrom and R. L. Beyer and were prepared and analyzed by R. L. Beyer. Collection locations with a map are given in Appendix I.

Thin section blocks were sawed and weathered pieces and saw marks removed by chipping them from the samples. The samples were broken with a hammer and pneumatic jack, crushed in a large iron jaw crusher, and then crushed in a small alumina-plate jaw crusher, yielding about 200 to 300 grams of coarsely crushed sample. The samples were then split with about 60 grams being set aside for fine grinding in preparation for X-ray fluorescence analyses (XRF). One gram of the coarse ground sample was used for instrumental neutron activation analyses (INAA).

X-ray fluorescence techniques as described by Norrish and Hutton (1969) were used for analyses of most major and minor elements reported here as oxides. Duplicate rock samples were analyzed. The raw data were normalized to 100% total oxides. Iron is calculated as Fe_2O_3 in the raw data, but FeO is reported and is used for calculations in models discussed in this dissertation. Sodium data were obtained by INAA. Differences in duplicate analyses were within error

limits as stated by Norrish and Hutton except for some silica data. Generally relative errors for FeO, MnO, K_2O, and P_2O_5 are less than 2%, those for SiO_2 and MgO are less than 3%, and errors for TiO_2, CaO, and Al_2O_3 are less than 4%. For rocks with particularly low abundances of an oxide, the errors may approach 10 or 20% due to physical limitations such as peak counts in relation to background and instrumental difficulties involved in the experiments. The results of the XRF analyses and the norms calculated from them (see Appendix II) are found in Tables 1a through 1f. Graphical representation for all data in the form of variation (Harker) diagrams is presented in Figures 3a through 3d.

Instrumental neutron activation analyses techniques described by Gordon, et al. (1968) were used to analyze the samples for sodium, iron, and trace elements. Inter-experimental values for the INAA data obtained were normalized to standard rocks, the values of which are reported with the data in Table 1f. Generally errors are less than 2% for Na, La, Sm, Eu, Fe, Co, and Sc, less than 5% for Tb, Yb, Lu, Th, Hf, Ta, and Cr, and less than 10% for Rb, Ba, and Ce.

Iron analyses were obtained by both INAA and XRF methods. Figure 4 shows a graphical comparison of the analyses obtained. The analyses are in good agreement although XRF methods yield slightly high iron values for high-iron rocks and slightly low iron values for low-iron rocks when compared to values obtained by INAA techniques.

Table 1a. Chemical Analyses and Molecular Norms.

Sample Name	Basalt-Andesites SP-1	RS	SSF-F	BB-5	FU-B[1]	FI-B	LR-1[1]	DG-2[1]	LCF-F[1]	RE-B	ILB[1]	PPCC-1[1]
Major elements as oxides (%)												
SiO_2	51.0	51.8	52.6	52.9	52.9	52.9	53.2	53.3	53.3	53.4	53.4	53.5
TiO_2	1.33	1.27	1.42	0.93	1.35	1.56	1.24	1.37	1.23	1.10	1.15	1.37
Al_2O_3	16.9	17.7	16.4	19.1	17.3	16.7	17.0	17.3	17.0	18.7	17.2	17.2
FeO*	8.87	7.60	8.87	6.87	8.22	8.81	8.16	8.10	8.13	7.87	7.59	8.22
MnO	0.17	0.14	0.17	0.13	0.16	0.17	0.16	0.16	0.15	0.15	0.15	0.15
MgO	6.16	6.19	5.48	5.77	5.28	5.08	5.40	4.92	5.54	5.22	5.41	5.12
CaO	10.25	9.68	9.41	9.66	9.28	9.10	9.13	8.70	9.07	8.95	9.18	8.48
Na_2Oaa	3.41	3.36	3.54	3.12	3.48	3.57	3.68	3.75	3.54	3.00	3.57	3.77
K_2O	0.64	0.97	0.86	0.58	0.84	0.87	0.90	1.05	0.90	0.60	1.20	0.96
P_2O_5	0.26	0.43	0.29	0.18	0.32	0.38	0.26	0.38	0.25	0.22	0.31	0.37
Loss	0.25	0.69	0.37	0.81	0.54	0.71	0.44	0.51	0.45	1.12	0.27	0.49
Minor and trace elements (ppm except as noted)												
Na (%)	2.52	2.45	2.62	2.31	2.55	2.62	2.74	2.73	2.61	2.19	3.63	2.79
Rb	--	--	--	--	--	d	--	--	--	--	d	--
Cs	--	--	--	--	d	--	d	d	d	--	d	--
Ba	--	530.	300.	300.	--	460.	270.	460.	300.	460.	550.	380.
La	10.	21.	12.	8.	14.	15.	11.	17.	12.	11.	18.	19.
Ce	--	45.	21.	18.	25.	27.	23.	37.	22.	22.	37.	37.
Nd	--	--	--	--	--	--	--	28.	d	--	38.	--
Sm	4.7	6.0	4.3	3.2	4.3	4.8	4.4	5.7	4.0	4.4	5.2	5.6
Eu	1.41	1.75	1.51	1.05	1.56	1.67	1.32	1.70	1.38	1.40	1.52	1.83
Tb	0.6	0.6	0.7	0.4	0.7	0.7	0.6	0.8	0.5	0.6	0.6	0.8
Yb	2.2	1.6	2.4	1.4	2.3	2.6	2.3	2.5	2.2	2.2	2.2	2.8
Lu	0.30	0.31	0.35	0.26	0.32	0.37	0.39	0.45	0.34	0.31	0.45	0.39
Th	1.5	2.7	1.5	0.9	2.0	1.9	2.0	2.1	2.2	1.0	3.0	2.0
Zr	--	--	--	--	--	--	--	--	--	--	--	--
Hf	2.2	3.1	2.9	2.0	3.0	3.2	2.6	3.7	3.0	2.4	3.3	3.8
Ta	0.5	0.4	0.6	0.3	0.6	0.5	0.3	0.6	0.5	0.2	0.5	0.5
Fe (%)	6.59	5.92	6.63	5.53	6.78	6.75	6.17	6.20	6.24	6.22	5.80	6.33
Co	35.1	31.1	31.4	31.2	33.0	29.0	31.2	28.3	31.0	30.9	28.6	28.3
Sc	34.8	27.1	34.0	26.7	34.0	33.0	30.3	27.0	30.8	29.8	27.3	28.6
Cr	140.	117.	89.	133.	106.	81.	113.	88.	111.	137.	88.	77.

MOLECULAR NORMS#

Sample Name	SP-1	RS	SSF-F	BB-5	FU-B[1]	FI-B	LR-1[1]	DG-2[1]	LCF-F[1]	RE-B	ILB[1]	PPCC-1[1]
QZ	--	--	0.10	1.63	1.14	1.26	0.34	0.91	1.03	3.94	0.33	1.20
OR	3.78	5.73	5.08	3.48	4.96	5.14	5.31	6.20	5.31	3.48	7.09	5.67
AB	28.85	28.43	29.95	26.65	29.44	30.20	31.13	31.73	29.95	25.38	30.20	31.90
AN	28.91	30.26	26.34	36.34	29.02	26.83	27.10	27.38	27.70	35.76	27.30	27.06
DI	16.57	12.17	15.15	8.71	12.24	13.02	13.52	10.92	12.83	6.14	13.26	10.33
HY	9.45	14.39	17.27	18.81	17.35	17.02	17.11	16.87	17.75	20.18	16.56	17.83
WO	8.44	6.24	7.70	4.46	6.23	6.60	6.88	5.55	6.53	3.12	6.76	5.25
EN	10.15	12.62	13.64	14.12	13.15	12.65	13.44	12.25	13.79	13.05	13.47	12.75
FS	7.42	7.69	11.07	8.93	10.21	10.78	10.30	9.99	10.24	10.15	9.58	10.16
OL	6.56	3.26	--	--	--	--	--	--	--	--	--	--
FO	3.63	1.95	--	--	--	--	--	--	--	--	--	--
FA	2.93	1.31	--	--	--	--	--	--	--	--	--	--
MT	1.86	1.59	1.86	1.45	1.72	1.85	1.71	1.70	1.70	1.66	1.59	1.72
IL	2.52	2.41	2.69	1.78	2.56	2.92	2.35	2.60	2.33	2.12	2.18	2.60
AP	0.61	1.01	0.68	0.45	0.75	0.90	0.61	0.90	0.59	0.54	0.73	0.87
CO	--	--	--	--	--	--	--	--	--	--	--	--

* Total Fe recalculated As FeO
aa Calculated from INAA Na data
d Detected but below limits for accurate determination
1 Samples used in average for Pri-Mag, see Table 4
See Appendix II for explanation of molecular norms

Table 1b. Chemical Analyses and Molecular Norms.

Sample Name	Basalt-Andesites DH-B	CH-B	CH-F	NS-1	LC-1	LP-F	SU-F	F-1	B10-1	MB-1	EPF-2	TV-F
Major elements as oxides (%)												
SiO_2	53.9	54.5	54.5	54.7	54.8	55.6	55.7	55.8	55.8	56.1	57.4	57.5
TiO_2	1.24	1.25	1.24	1.26	1.21	0.99	1.16	1.27	1.53	1.26	1.42	1.22
Al_2O_3	17.1	17.0	16.9	16.6	16.6	17.3	16.4	16.4	16.1	15.8	15.8	15.6
FeO*	7.47	7.86	7.91	8.02	7.78	6.53	7.42	7.82	8.52	8.08	8.00	7.70
MnO	0.14	0.15	0.15	0.16	0.16	0.14	0.14	0.15	0.16	0.16	0.15	0.15
MgO	5.11	4.86	4.73	4.84	5.02	5.07	4.90	4.23	3.67	4.42	3.35	4.09
CaO	8.90	8.43	8.47	8.43	8.37	8.13	7.83	7.69	7.29	7.64	6.56	7.10
Na_2O**	3.70	3.97	4.03	3.80	3.84	3.69	3.96	4.15	4.19	3.91	4.38	3.86
K_2O	1.25	0.89	0.90	1.12	1.13	1.52	1.42	1.38	1.43	1.56	1.72	1.67
P_2O_5	0.40	0.24	0.23	0.26	0.25	0.29	0.27	0.28	0.40	0.20	0.34	0.21
Loss	0.47	0.43	0.35	0.39	0.43	0.53	0.38	0.38	0.40	0.29	0.07	0.60
Minor and trace elements (ppm except as noted)												
Na (%)	2.73	2.73	2.97	2.79	2.84	2.71	2.92	3.02	3.14	2.89	3.27	2.85
Rb	—	—	—	—	—	d	—	—	—	—	40.	d
Cs	—	d	d	d	0.9	1.0	1.1	1.1	1.0	1.4	1.2	1.5
Ba	610.	340.	360.	430.	330.	610.	400.	440.	410.	470.	600.	500.
La	22.	11.	11.	14.	13.	21.	15.	15.	20.	15.	21.	16.
Ce	39.	21.	22.	24.	27.	41.	32.	33.	40.	30.	41.	29.
Nd	—	—	—	—	25.	—	—	—	23.	—	30.	—
Sm	6.2	4.3	4.2	5.0	4.8	5.9	5.2	5.4	6.5	5.1	5.9	5.0
Eu	1.72	1.40	1.41	1.50	1.42	1.57	1.44	1.61	1.88	1.37	1.77	1.40
Tb	0.6	0.6	0.6	0.8	0.7	0.7	0.7	0.7	0.8	0.7	0.9	0.8
Yb	2.2	2.4	2.2	2.5	2.4	2.4	2.6	2.9	3.0	3.0	3.0	3.4
Lu	0.39	0.36	0.39	0.39	0.42	0.43	0.47	0.50	0.44	0.59	0.54	0.59
Th	3.6	1.8	1.8	2.7	2.8	4.4	3.8	3.6	2.3	4.2	4.4	4.9
Zr	—	—	—	—	—	—	—	—	—	—	110.	—
Hf	4.0	2.5	2.2	3.5	3.2	4.1	3.8	3.9	4.5	3.6	4.6	4.2
Ta	0.4	—	0.2	0.5	0.6	0.6	0.7	0.7	0.7	0.7	1.9	0.8
Fe (%)	5.75	5.90	5.89	6.16	6.07	4.90	5.57	6.01	6.61	6.15	5.90	5.95
Co	26.8	26.1	26.7	28.0	29.0	24.9	26.0	25.3	24.0	29.1	20.3	27.1
Sc	27.6	28.5	28.5	29.7	29.0	22.9	26.3	27.8	28.0	29.8	24.5	28.1
Cr	88.	82.	84.	89.	107.	92.	104.	69.	26.	48.	20.	44.

MOLECULAR NORMS#

Sample Name	DH-B	CH-B	CH-F	NS-1	LC-1	LP-F	SU-F	F-1	B10-1	MB-1	EPF-2	TV-F
QZ	1.08	1.95	1.84	2.43	2.18	2.61	2.74	3.07	3.96	3.76	5.40	6.46
OR	7.38	5.25	5.31	6.61	6.67	9.02	8.39	8.15	8.45	9.21	10.24	9.86
AB	31.30	33.59	34.10	32.15	32.49	31.36	33.50	35.11	35.45	33.08	37.34	32.66
AN	26.33	25.96	25.33	24.84	24.77	26.27	22.75	21.90	20.89	20.87	18.56	20.38
DI	12.45	11.74	12.70	12.56	12.40	10.07	11.75	11.89	10.51	12.97	9.91	11.11
HY	15.86	16.14	15.34	15.92	16.20	16.07	15.74	14.39	14.26	14.75	13.29	14.33
WO	6.35	5.96	6.44	6.37	6.31	5.15	5.98	6.01	5.28	6.56	4.97	5.62
EN	12.72	12.10	11.58	12.05	12.50	12.68	12.20	10.53	9.14	11.00	8.40	10.18
FS	9.24	9.81	10.02	10.05	9.79	8.31	9.31	9.73	10.35	10.15	9.82	9.64
OL	—	—	—	—	—	—	—	—	—	—	—	—
FO	—	—	—	—	—	—	—	—	—	—	—	—
FA	—	—	—	—	—	—	—	—	-	—	—	—
MT	1.57	1.65	1.67	1.68	1.63	1.37	1.56	1.64	1.79	1.69	1.69	1.61
IL	2.35	2.37	2.37	2.39	2.29	1.88	2.20	2.41	2.90	2.39	2.71	2.31
AP	0.94	0.56	0.54	0.61	0.59	0.69	0.64	0.66	0.94	0.47	0.83	0.49
CO	—	—	—	—	—	—	—	—	—	—	—	—

* Total Fe recalculated as FeO
** Calculated from INAA Na data
d Detected but below limits for accurate determination
See Appendix II for explanation of molecular norms

Table 1c. Chemical Analyses and Molecular Norms.

	Basalt-Andesites						High-Iron Basalts					
Sample Name	FI-8	LB-3+	LB-2+	LB-4+	LB-5+	LB-1+	DG-1[2]	NPP-3[2]	NPP-2[2]	F-2[2]	A2-3[2]	NPP-1[2]
Major elements as oxides (%)												
SiO_2	57.6	54.5	55.0	56.0	56.0	56.4	52.2	52.3	52.5	52.5	52.5	52.5
TiO_2	1.02	1.06	1.13	1.13	1.08	1.07	2.09	2.36	2.36	2.17	2.24	2.33
Al_2O_3	16.9	15.6	16.0	16.1	15.8	16.4	15.6	15.3	15.4	15.4	15.4	15.2
FeO*	6.75	7.6	7.7	7.7	7.6	7.2	10.67	11.27	11.16	10.92	10.90	11.24
MnO	0.14	0.13	0.13	0.14	0.13	0.14	0.21	0.21	0.20	0.20	0.20	0.21
MgO	4.14	4.57	4.52	4.49	4.71	4.36	4.19	3.77	3.80	3.96	3.89	3.83
CaO	6.91	8.0	8.1	8.2	8.1	7.7	8.38	7.74	7.77	8.05	8.00	7.72
Na_2O**	4.18	3.59	3.62	3.72	3.88	3.79	4.08	4.48	4.29	4.23	4.30	4.33
K_2O	1.39	1.30	1.19	1.25	1.32	1.42	0.99	0.87	0.84	0.97	0.87	0.90
P_2O_5	0.24	—	—	—	—	—	0.42	0.45	0.47	0.43	0.44	0.46
Loss	0.52	—	—	—	—	—	0.20	0.20	0.42	0.09	0.16	0.19
Minor and trace elements (ppm except as noted)												
Na (%)	3.08	2.90	2.93	2.90	2.93	2.98	3.03	3.29	3.15	3.14	3.19	3.18
Rb	d	39.	—	33.	32.	—	—	—	—	—	—	—
Cs	1.3	1.1	—	1.1	1.1	1.0	—	—	—	—	—	—
Ba	640.	340.	390.	450.	390.	400.	330.	430.	350.	440.	300.	350.
La	16.	14.	14.	14.	14.	14.	15.	15.	15.	16.	15.	16.
Ce	28.	29.	29.	31.	30.	31.	31.	30.	28.	33.	32.	25.
Nd	—	—	—	—	—	—	—	—	—	32.	—	—
Sm	5.2	4.7	4.6	4.9	4.7	5.0	6.5	6.0	6.3	6.2	6.4	6.4
Eu	1.73	1.37	1.20	1.48	1.39	1.11	2.06	2.24	2.30	2.20	2.08	2.23
Tb	0.8	0.6	0.7	0.6	0.6	0.7	0.9	1.0	1.1	1.1	1.0	1.0
Yb	3.9	2.8	2.7	2.5	2.5	2.7	3.4	3.6	3.7	3.7	3.4	3.8
Lu	0.48	0.43	0.45	0.42	0.47	0.44	0.62	0.55	0.61	0.57	0.58	0.57
Th	3.3	3.6	3.4	3.4	3.5	3.7	1.6	1.5	1.5	1.6	1.4	1.1
Zr	—	—	—	—	—	—	—	130.	—	—	—	—
Hf	4.1	3.5	3.7	3.7	3.9	3.8	3.9	4.1	4.1	4.5	3.9	4.0
Ta	0.5	0.7	—	0.7	0.7	0.5	0.7	0.7	0.6	0.8	0.6	0.6
Fe (%)	5.16	5.48	5.61	5.73	5.62	5.65	8.07	8.66	8.57	8.36	8.38	8.66
Co	21.8	27.9	27.7	27.6	27.9	26.9	32.2	30.3	30.2	30.9	31.5	30.7
Sc	22.2	25.3	25.8	25.7	25.7	25.8	35.9	35.4	35.2	34.1	35.6	35.5
Cr	77.	114.	107.	107.	111.	100.	23.	—	—	d	d	—

MOLECULAR NORMS#

Sample Name	FI-8	LB-3+	LB-2+	LB-4+	LB-5+	LB-1+	DG-1[2]	NPP-3[2]	NPP-2[2]	F-2[2]	A2-3[2]	NPP-1[2]
QZ	5.79	4.12	4.52	4.59	3.63	5.11	—	—	0.77	—	0.23	0.35
OR	8.21	7.96	7.21	7.47	7.90	8.52	5.85	5.14	4.96	5.73	5.14	5.31
AB	35.28	31.50	31.43	31.83	33.26	32.56	34.52	37.90	36.30	35.79	36.38	36.63
AN	23.39	23.45	24.51	23.80	22.08	23.90	21.27	19.17	20.14	20.14	20.25	19.46
DI	7.65	14.57	13.76	14.28	15.31	11.82	14.62	13.62	12.82	14.18	13.82	13.24
HY	15.08	14.64	14.69	14.20	14.10	14.46	14.57	13.64	16.00	15.64	15.54	16.05
WO	3.88	7.39	6.98	7.23	7.77	6.00	7.33	6.79	6.40	7.09	6.91	6.61
EN	10.31	11.80	11.55	11.30	11.88	11.02	9.86	8.53	9.46	9.84	9.68	9.53
FS	8.54	10.01	9.92	9.93	9.75	9.26	12.00	11.93	12.95	12.89	12.76	13.14
OL	—		—	—	—	—	0.94	1.52	—	0.03	—	—
FO	—	—	—	—	—	—	0.40	0.59	—	0.01	—	—
FA	—	—	—	—	—	—	0.54	0.92	—	0.02	—	—
MT	1.41	1.64	1.65	1.64	1.61	1.53	2.24	2.36	2.34	2.29	2.29	2.36
IL	1.93	2.08	2.20	2.17	2.07	2.06	3.96	4.48	4.48	4.12	4.25	4.42
AP	0.56	—	—	—	—	—	0.99	1.06	1.11	1.01	1.04	1.09
CO	—	—	—	—	—	—	—	—	—	—	—	—

* Total Fe recalculated as FeO
** Calculated from INAA Na data
d Detected but below limits for accurate determination
\+ Major element analyses by William P. Leeman
2 Samples used in average for Pre-Bas, see Table 4
See Appendix II for explanation of molecular norms

Table 1d. Chemical Analyses and Molecular Norms.

	Amota Butte							Rhyolites				
Sample Name	AM-6[3]	AM-5[3]	AM-8[3]	AM-7[3]	AM-1[3]	AM-3[3]	AM-2[3]	FF-6[4]	FF-9[4]	FF-5[4]	FF-4[4]	FF-7[4]
Major elements as oxides (%)												
SiO_2	63.0	64.1	64.4	64.7	65.2	65.5	65.7	71.2	71.4	71.4	71.5	71.5
TiO_2	0.93	0.88	0.86	0.88	0.84	0.83	0.82	0.33	0.34	0.32	0.34	0.31
Al_2O_3	16.6	16.4	16.4	16.4	15.8	15.9	15.9	14.7	14.7	14.4	14.8	14.5
FeO*	5.64	5.34	5.16	5.24	4.82	4.89	4.77	2.77	2.74	2.62	2.70	2.65
MnO	0.15	0.16	0.16	0.15	0.15	0.13	0.12	0.11	0.09	0.09	0.16	0.09
MgO	1.51	1.25	1.20	0.96	1.06	1.06	0.98	0.47	0.27	0.63	0.30	0.36
CaO	4.12	3.72	3.72	3.49	3.04	2.84	2.87	1.19	1.14	1.17	1.19	1.13
Na_2O**	4.86	4.93	5.00	4.96	5.25	5.51	5.43	5.91	5.96	6.03	5.70	6.04
K_2O	2.28	2.37	2.36	2.46	3.03	2.60	2.57	2.97	3.03	3.07	3.02	3.04
P_2O_5	0.27	0.25	0.26	0.25	0.24	0.25	0.25	0.05	0.04	0.04	0.04	0.03
Loss	0.74	0.60	0.50	1.09	0.62	0.79	0.82	0.37	0.30	0.21	0.37	0.17
Minor and trace elements (ppm except as noted)												
Na (%)	3.56	3.62	3.66	3.67	3.82	4.03	4.03	4.36	4.39	4.47	4.23	4.49
Rb	45.	55.	74.	63.	--	--	--	67.	75.	71.	70.	71.
Cs	1.9	1.2	1.2	1.6	--	2.6	--	2.3	2.3	2.5	2.3	0.9
Ba	870.	930.	840.	870.	980.	960.	950.	1020.	980.	860.	1040.	860.
La	22.	23.	23.	21.	27.	25.	24.	28.	27.	27.	28.	28.
Ce	41.	41.	41.	46.	43.	46.	42.	49.	59.	54.	--	49.
Nd	--	32.	--	--	--	33.	35.	38.	35.	33.	34.	37.
Sm	7.2	7.4	6.1	7.0	8.5	7.4	8.0	7.3	8.1	7.4	7.8	7.5
Eu	1.86	2.07	1.85	1.77	2.06	1.90	1.82	1.57	1.57	1.47	1.49	1.51
Tb	1.1	1.1	1.0	0.9	1.2	0.9	1.2	1.3	1.4	1.1	1.2	1.1
Yb	3.3	4.6	3.7	3.8	4.4	3.8	3.7	5.3	5.7	4.9	5.6	4.8
Lu	0.58	0.68	0.63	0.66	0.79	0.66	0.70	0.77	0.82	0.80	0.78	0.78
Th	6.9	6.9	7.3	6.8	5.2	5.9	5.4	7.6	7.8	7.4	7.6	7.5
Zr	170.	--	--	190.	--	--	--	280.	320.	290.	270.	320.
Hf	4.8	5.1	5.0	4.9	6.0	5.8	5.8	8.5	8.7	7.9	8.8	8.1
Ta	0.7	0.6	0.6	0.5	--	--	--	1.0	1.0	1.2	1.0	1.2
Fe (%)	4.33	4.24	3.91	4.06	3.69	3.61	3.68	2.06	2.14	2.01	2.09	1.97
Co	8.9	8.5	7.9	8.2	4.2	4.1	4.1	0.8	0.8	0.7	0.8	0.7
Sc	16.6	16.2	15.0	15.6	14.2	14.8	14.4	9.20	9.39	9.02	9.36	9.06
Cr	--	5.	--	4.	--	--	--	5.	--	1.	2.	--

MOLECULAR NORMS#

Sample Name	AM-6[3]	AM-5[3]	AM-8[3]	AM-7[3]	AM-1[3]	AM-3[3]	AM-2[3]	FF-6[4]	FF-9[4]	FF-5[4]	FF-4[4]	FF-7[4]
QZ	24.62	14.47	14.58	15.33	13.52	14.10	14.93	20.75	20.96	20.23	22.20	20.72
OR	13.74	14.00	13.94	14.53	17.90	15.36	15.18	17.55	17.90	18.18	17.84	18.01
AB	24.69	41.71	42.30	41.97	44.42	46.62	45.94	30.00	30.43	51.15	48.23	51.24
AN	19.05	15.51	15.19	15.11	10.67	10.83	11.53	4.91	4.38	3.02	5.64	3.56
DI	--	1.11	1.32	0.48	2.41	1.37	0.91	0.52	0.88	2.14	--	1.60
HY	11.05	9.28	8.82	8.70	7.42	8.04	7.88	4.65	3.86	3.99	4.47	3.64
WO	--	0.54	0.65	0.23	1.18	0.67	0.44	0.25	0.42	1.05	--	0.77
EN	3.83	3.11	2.98	2.39	2.64	2.64	2.44	1.17	0.67	1.57	0.74	0.89
FS	7.22	6.73	6.50	6.56	6.01	6.10	5.91	3.75	3.64	3.51	3.72	3.57
OL	--	--	--	--	--	--	--	--	--	--	--	--
FO	--	--	--	--	--	--	--	--	--	--	--	--
FA	--	--	--	--	--	--	--	--	--	--	--	--
MT	1.21	1.12	1.08	1.10	1.01	1.02	1.00	0.58	0.57	0.55	0.56	0.55
IL	1.80	1.67	1.63	1.67	1.59	1.57	1.55	0.62	0.64	0.60	0.64	0.59
AP	0.65	0.59	0.61	0.59	0.56	0.59	0.59	0.11	0.09	0.09	0.09	0.07
CO	2.61	--	--	--	--	--	--	--	--	--	0.03	--

* Total Fe recalculated as FeO
** Calculated from INAA Na data
d Detected but below limits for accurate determination
3 Samples used in average for AM-Avg, see Table 4.
4 Samples used in average for FF-Avg, see Table 4.
See Appendix II for explanation of molecular norms.

Table 1a. Chemical Analyses and Molecular Norms.

Sample Name	Rhyolites RS-3	PUMICE	RS-2	BOF	ILO	CH-3	CH-1	MC-2A	EAB-3	EAB-1	MC-2B
Major elements as oxides (%)											
SiO_2	71.9	72.5	72.7	73.2	73.6	73.6	73.8	74.3	74.5	74.9	74.9
TiO_2	0.37	0.30	0.29	0.26	0.26	0.20	0.23	0.25	0.17	0.16	0.25
Al_2O_3	14.5	14.2	14.2	14.0	13.8	13.7	13.9	13.6	13.7	13.8	13.4
FeO*	2.39	2.22	2.03	2.02	1.80	2.32	2.41	1.79	1.75	1.55	1.63
MnO	0.08	0.07	0.07	0.06	0.06	0.07	0.07	0.05	0.04	0.02	0.04
MgO	0.52	0.30	0.27	0.23	0.35	0.23	0.15	0.30	0.16	0.33	0.18
CaO	1.33	0.93	1.00	0.88	0.96	0.79	0.83	1.06	0.95	0.80	0.83
Na_2O**	5.09	5.19	5.03	5.07	4.71	5.02	4.76	4.30	4.63	4.20	4.40
K_2O	3.50	4.05	4.15	4.08	4.25	3.80	3.62	4.04	3.87	4.06	4.17
P_2O_5	0.06	0.03	0.03	0.02	0.03	0.01	0.01	0.04	0.01	0.02	0.02
Loss	0.19	2.23	0.50	0.13	0.14	0.64	0.61	0.69	0.25	0.69	0.35
Minor and trace elements (ppm except as noted)											
Na (%)	3.75	3.64	3.70	3.73	3.46	3.72	3.51	3.18	3.43	3.11	3.26
Rb	96.	112.	121.	113.	133.	105.	98.	127.	109.	120.	119.
Cs	4.0	4.5	4.5	4.2	5.0	2.8	2.9	4.8	2.9	4.2	2.2
Ba	1100.	1050.	940.	980.	1000.	1050.	1180.	1290.	1010.	1090.	1120.
La	27.	31.	30.	31.	30.	30.	31.	26.	24.	27.	23.
Ce	--	--	62.	--	--	53.	--	--	49.	--	51.
Nd	34.	34.	34.	35.	30.	39.	34.	21.	30.	30.	29.
Sm	6.6	6.7	7.7	6.7	6.6	8.6	7.4	5.1	6.3	5.2	5.4
Eu	1.24	0.98	0.82	0.92	0.79	1.27	1.33	0.71	0.86	0.83	0.58
Tb	1.0	1.1	1.4	1.2	1.0	1.4	1.0	0.7	0.8	0.8	0.6
Yb	4.6	5.6	5.5	4.7	4.9	5.1	5.2	3.6	4.2	3.2	3.4
Lu	0.69	0.78	0.95	0.76	0.74	0.90	0.81	0.61	0.77	0.45	0.61
Th	11.9	13.6	13.3	13.9	15.2	11.8	11.4	13.8	13.0	14.0	13.8
Zr	250.	350.	260.	230.	210.	260.	280.	150.	190.	190.	200.
Hf	8.1	9.1	8.7	9.0	4.7	8.0	9.1	6.5	5.6	6.0	5.9
Ta	1.1	1.4	1.2	1.5	1.2	0.8	0.9	0.9	0.8	0.8	0.8
Fe (%)	1.73	1.89	1.56	1.57	1.39	1.77	1.93	1.34	1.41	1.15	1.29
Co	1.8	2.3	1.4	0.9	1.2	0.8	1.0	1.5	0.4	0.4	1.3
Sc	7.85	7.78	5.99	6.36	5.36	9.91	11.37	5.16	6.08	4.47	5.00
Cr	2.	8.	--	--	2.	--	1.	--	2.	1.	2.

MOLECULAR NORMS#

Sample Name	RS-3	PUMICE	RS-2	BOF	ILO	CH-3	CH-1	MC-2A	EAB-3	EAB-1	MC-2B
QZ	23.97	23.22	24.05	25.12	26.47	26.49	28.73	30.19	29.43	31.88	30.39
OR	20.68	23.93	24.52	23.99	25.11	22.45	21.39	23.87	22.86	23.99	24.64
AB	43.07	43.91	42.56	42.90	39.85	42.47	40.27	36.38	39.17	35.53	37.23
AN	6.30	3.40	3.93	3.31	3.98	3.51	4.05	4.99	4.64	3.83	3.98
DI	--	0.87	0.71	0.80	0.49	0.29	--	--	--	--	--
HY	4.36	3.21	2.95	2.66	2.95	3.64	3.68	3.07	2.78	2.88	2.51
WO	--	0.42	0.34	0.38	0.24	0.14	--	--	--	--	--
EN	1.29	0.74	0.67	0.39	0.87	0.57	0.37	0.74	0.39	0.82	0.44
FS	3.07	2.91	2.65	2.68	2.34	3.22	3.31	2.32	2.38	2.05	2.06
OL	--	--	--	--	--	--	--	--	--	--	--
FO	--	--	--	--	--	--	--	--	--	--	--
FA	--	--	--	--	--	--	--	--	--	--	--
MT	0.50	0.46	0.42	0.42	0.37	0.48	0.50	0.37	0.36	0.32	0.34
IL	0.70	0.57	0.55	0.53	0.49	0.38	0.43	0.47	0.32	0.30	0.47
AP	0.14	0.07	0.07	0.04	0.07	0.02	0.02	0.09	0.02	0.04	0.04
CO	0.02	--	--	--	--	--	0.66	0.36	0.20	1.04	0.21

* Total Fe recalculated as FeO
** Calculated from INAA Na data
d Detected but below limits for accurate determination
\# See Appendix II for explanation of molecular norms.

Table 1f. Chemical Analyses and Molecular Norms.

Sample Name	Newberry Area Samples FS-8	FF-1	17	8	19	BRB-Q	FM-2	FM-1	FM-3	Standard Rocks W-1	BCR-1	GSP-1
Major elements as oxides (%)												
SiO_2	48.8	61.8	52.5	53.7	55.9	58.2	60.9	72.5	72.5			
TiO_2	1.03	1.33	1.28	1.22	0.80	0.85	0.76	0.33	0.30			
Al_2O_3	17.6	15.8	18.0	16.9	18.6	17.3	16.6	14.8	14.6			
FeO*	9.09	6.15	7.86	8.02	6.23	6.16	5.84	2.43	2.24			
MnO	0.17	0.18	0.15	0.15	0.12	0.13	0.12	0.05	0.06			
MgO	8.06	2.10	5.21	6.41	4.62	4.18	3.60	0.43	0.78			
CaO	10.80	4.23	9.18	7.96	8.20	7.21	6.28	2.94	3.12			
Na_2O**	2.90	5.78	3.79	3.58	3.75	3.97	3.57	3.42	3.34			
K_2O	0.36	1.51	0.85	0.94	0.97	1.20	1.60	2.77	2.69			
P_2O_5	0.25	0.52	0.36	0.23	0.15	0.21	0.18	0.09	0.09			
Loss	0.31	0.58	0.23	0.25	0.46	0.33	0.84	1.28	0.42			
Minor and trace elements (ppm except as noted)												
Na (%)	2.15	4.29	2.81	2.67	2.78	2.93	2.66	2.49	2.50	1.63	2.41	1.17
Rb	--	d	d	--	d	d	d	65.	73.	d	49.	253.
Cs	--	d	--	d	d	d	d	1.4	1.7	1.0	0.9	0.9
Ba	--	500.	340.	270.	300.	380.	830.	1210.	1100.	160.	710.	1380.
La	7.	19.	17.	11.	11.	14.	16.	21.	19.	11.	25.	178.
Ce	14.	43.	34.	22.	19.	29.	31.	39.	37.	23.	46.	404.
Nd	--	38.	19.	--	d	--	--	19.	30.	18.	37.	267.
Sm	3.2	7.6	5.1	3.1	2.8	3.6	4.1	3.2	3.3	3.7	7.0	26.0
Eu	1.12	2.41	1.61	1.33	1.00	1.14	1.12	0.78	0.70	1.04	2.06	2.39
Tb	0.5	1.1	0.6	0.5	0.4	0.5	0.3	0.2	0.3	0.5	1.0	1.3
Yb	2.3	3.9	2.1	2.0	1.4	1.6	1.6	1.5	2.0	2.0	3.3	1.3
Lu	0.42	0.63	0.34	0.36	0.24	0.26	0.34	0.22	0.37	0.37	0.56	0.25
Th	0.7	3.3	1.3	2.1	1.8	2.2	3.1	7.3	8.4	2.4	6.7	122.0
Zr	--	210.	140.	--	140.	120.	--	150.	--	--	190.	450.
Hf	1.8	4.9	3.4	3.0	2.1	2.8	3.2	3.6	3.3	2.2	4.6	14.5
Ta	0.9	0.8	0.7	0.4	0.4	0.4	0.2	0.5	0.2	0.5	0.7	0.9
Fe (%)	6.81	4.65	5.68	5.66	4.60	4.45	4.36	1.79	1.71	7.73	9.37	2.95
Co	43.4	6.2	21.6	34.2	25.0	21.1	21.1	4.4	4.8	45.8	37.6	6.64
Sc	34.8	19.3	23.9	23.5	18.7	16.5	17.3	5.81	5.85	38.0	34.1	6.25
Cr	188.	1.5	71.	212.	58.	44.	6.	4.	10.	118.	10.	14.

MOLECULAR NORMS#

Sample Name	FS-8	FF-1	17	8	19	BRB-Q	FM-2	FM-1	FM-3
QZ	--	9.49	--	1.10	4.54	7.68	13.39	33.85	33.88
OR	2.12	8.91	5.06	5.59	5.76	7.13	9.45	16.36	15.90
AB	24.53	49.20	32.31	30.53	31.92	33.79	30.20	28.93	28.27
AN	33.80	12.70	29.76	27.37	31.18	25.85	24.40	13.99	14.89
DI	14.76	4.17	11.27	8.89	7.16	7.17	4.58	--	--
HY	4.79	10.44	14.57	21.93	16.21	14.94	14.30	4.20	4.83
WO	7.57	2.08	5.74	4.55	3.65	3.65	2.32	--	--
EN	7.49	5.26	11.47	16.08	11.57	10.47	8.96	1.07	1.94
FS	4.49	7.27	8.63	10.18	8.14	7.99	7.59	3.13	2.88
OL	14.64	--	2.05	--	--	--	--	--	--
FO	8.81	--	1.12	--	--	--	--	--	--
FA	5.82	--	0.93	--	--	--	--	--	--
MT	1.91	1.30	1.66	1.69	1.31	1.30	1.22	0.51	0.46
IL	1.95	2.54	2.45	2.33	1.52	1.62	1.44	0.62	0.57
AP	0.59	1.23	0.85	0.48	0.35	0.50	0.42	0.21	0.21
CO	--	--	--	--	--	--	--	1.05	0.76

* Total Fe recalculated as FeO
** Calculated from INAA Na data
d Detected but below limits for accurate determination
See Appendix 11 for explanation of molecular norms.

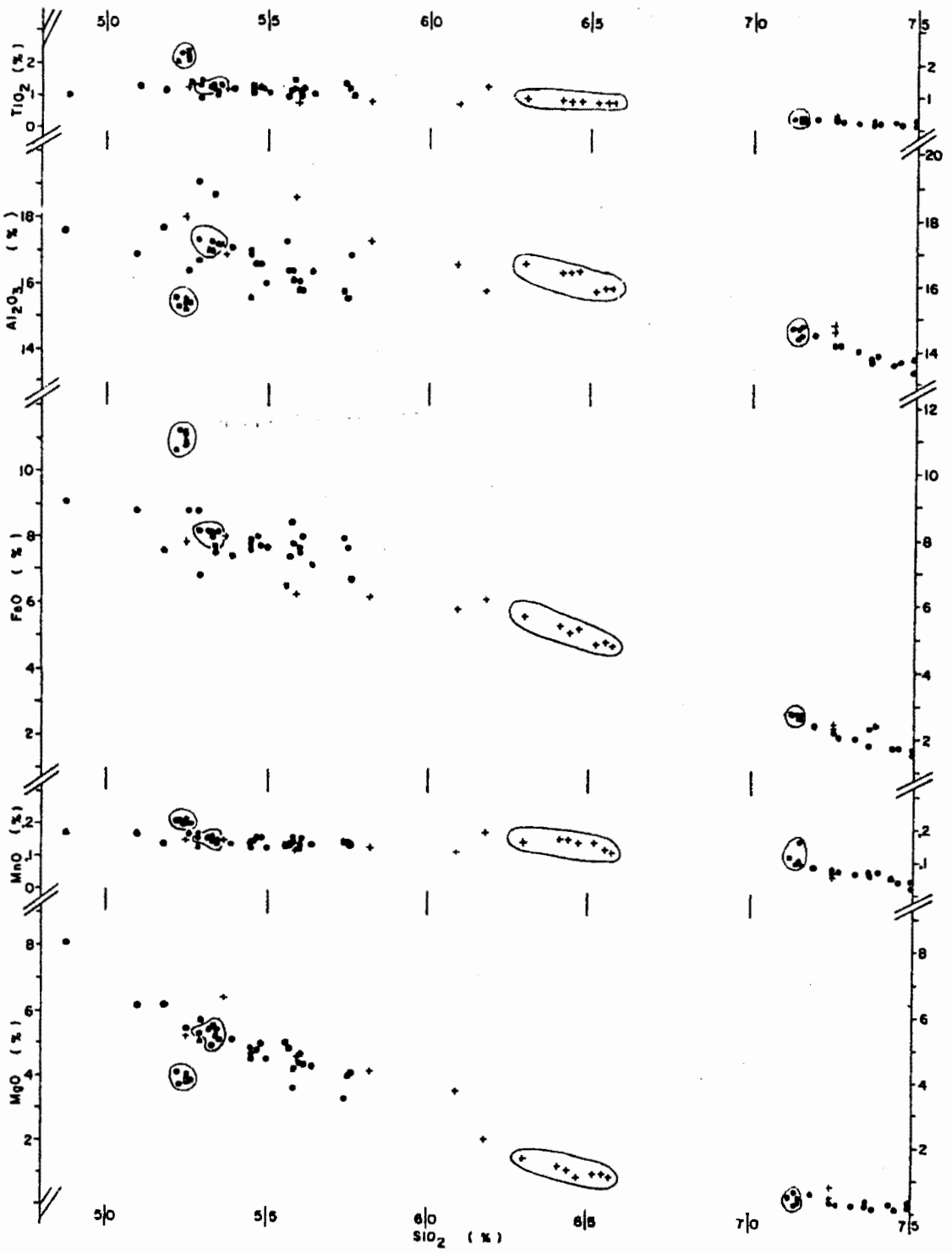

Figure 3a. Variation Diagrams of Chemical Analyses. Dots represent Newberry Suite samples, crosses represent other samples from the area, and circled groups of samples show groupings used in some interpretations.

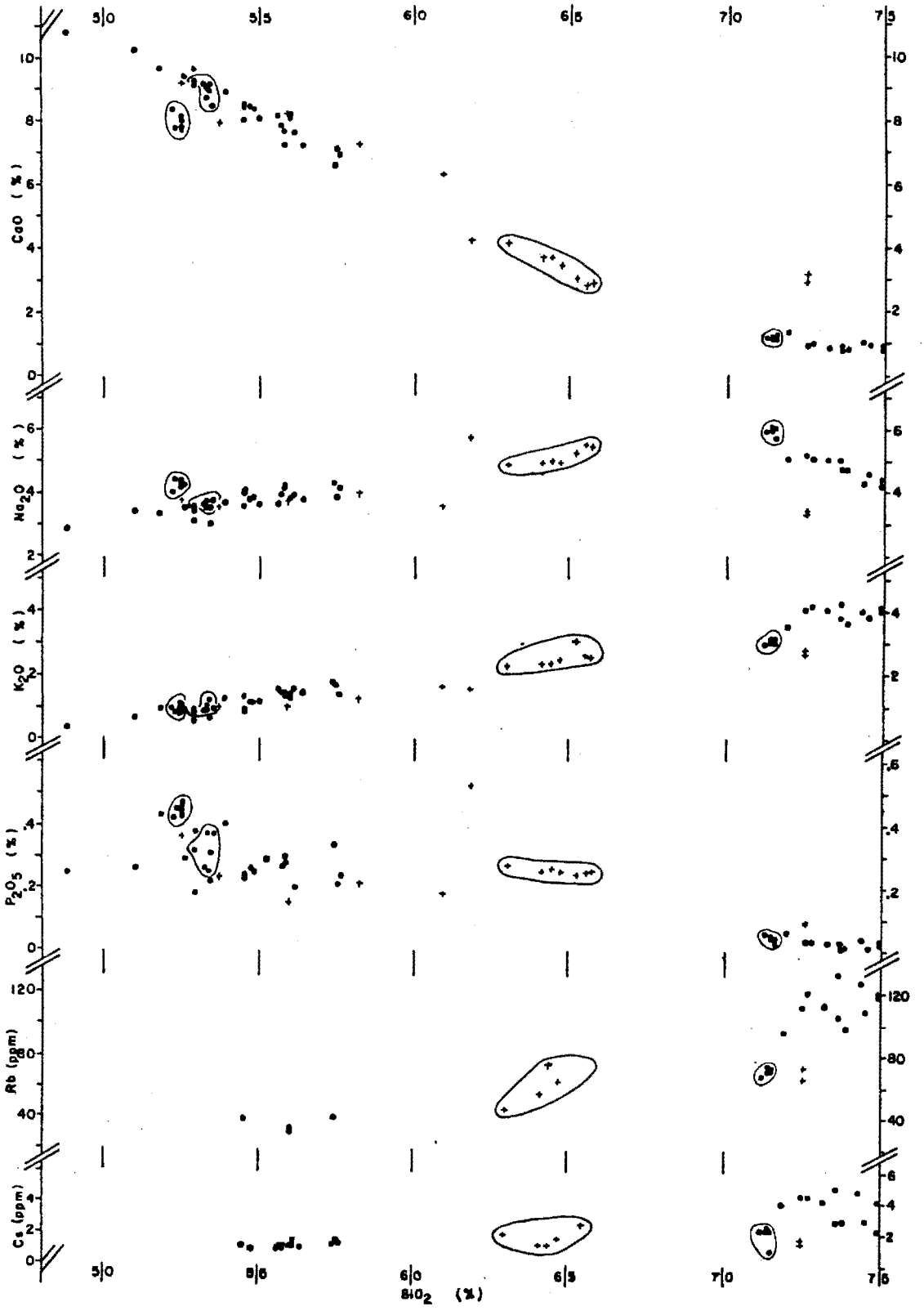

Figure 3b. Variation Diagrams of Chemical Analyses. Dots represent Newberry Suite samples, crosses represent other samples from the area, and circled groups of samples show groupings used in some interpretations.

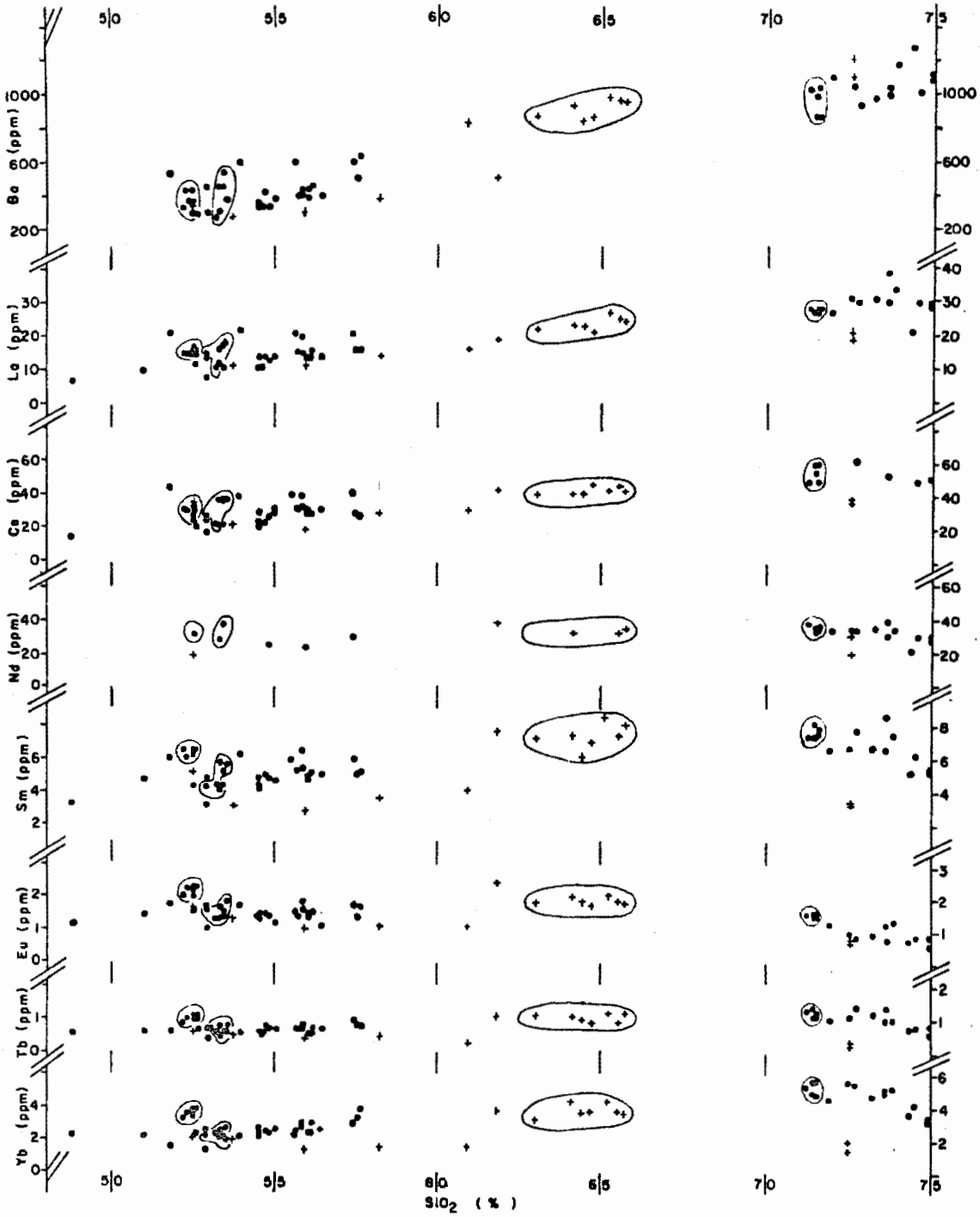

Figure 3c. Variation Diagrams of Chemical Analyses. Dots represent Newberry Suite samples, crosses represent other samples from the area, and circled groups of samples show groupings used in some interpretations.

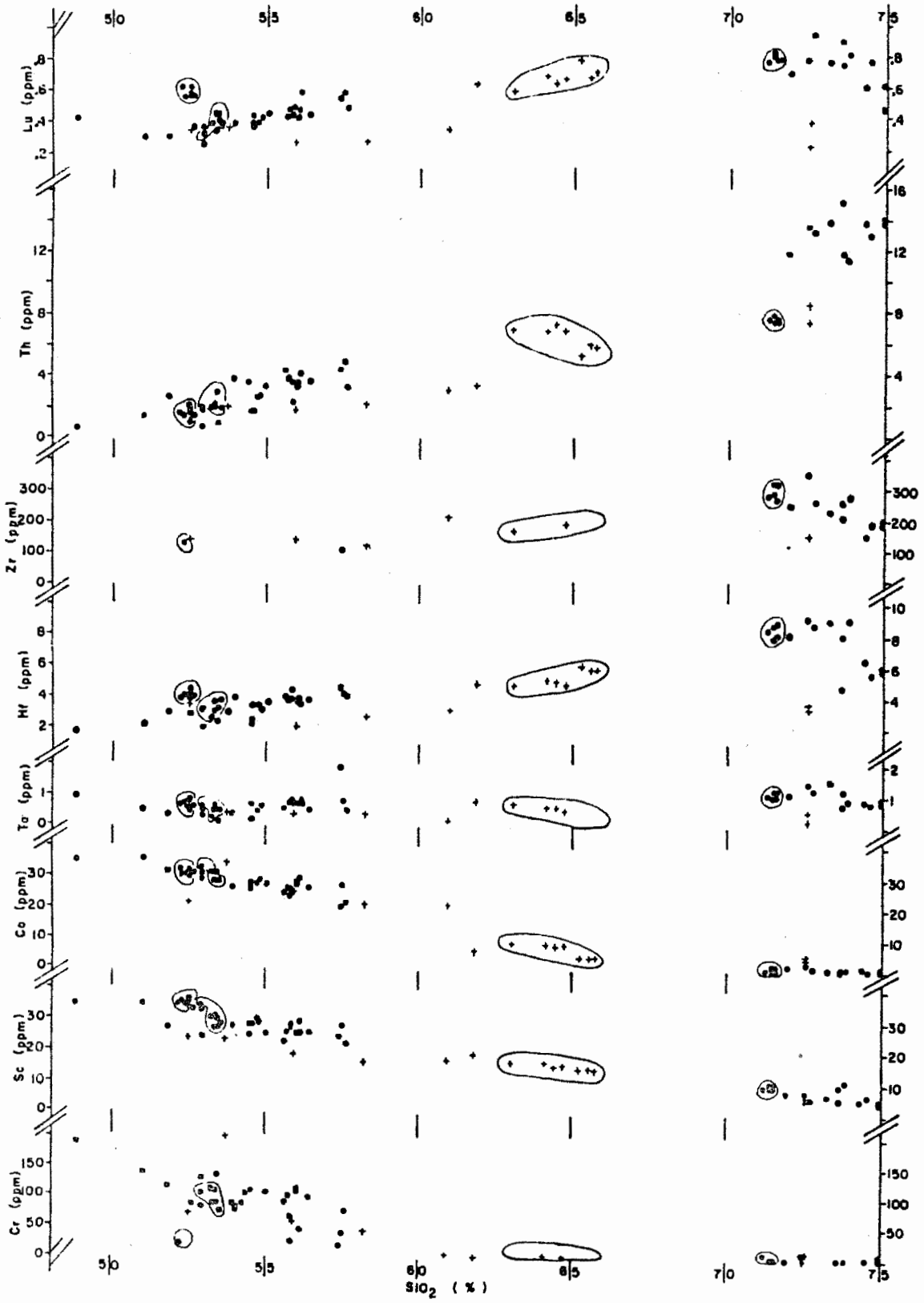

Figure 3d Variation Diagrams of Chemical Analyses. Dots represent Newberry Suite samples, crosses represent other samples from the area, and circled groups of samples show groupings used in some interpretations.

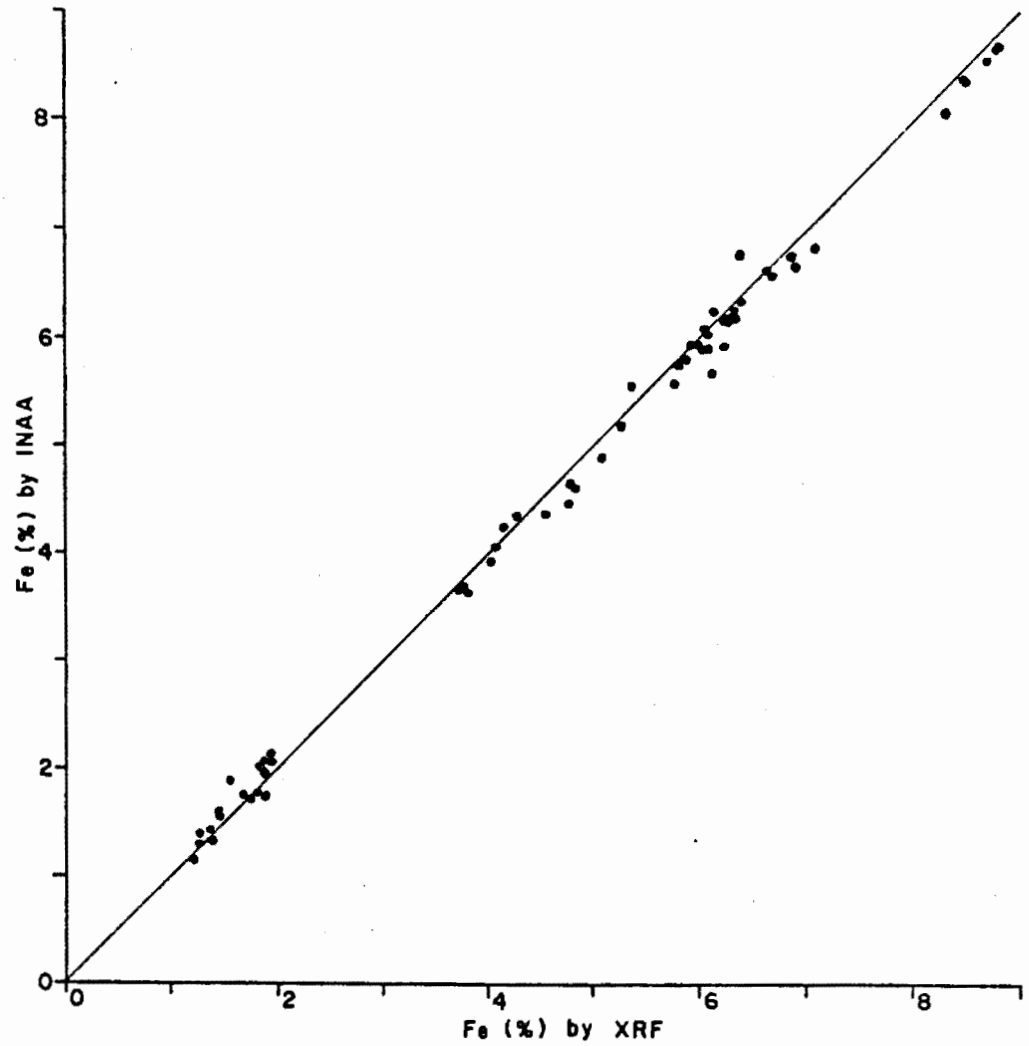

Figure 4. Comparison of Iron Values Obtained by XRF and INAA.

This slight discrepancy is probably due to errors in the matrix correction factors applied in the analyses using XRF techniques.

Sample Notes

All rocks in the area were assumed to be genetically related to the central complex with obvious exceptions to be stated later. Homogeneity of individual units was not tested, but the five pulses at Lava Butte are relatively uniform (see Table 1c, samples LB-1 thru LB-5) and the Big Obsidian Flow has been tested and is known to be of surprisingly uniform composition. As will be discussed in detail, most of the basaltic andesites have a consistent compositional variation and regardless of variations within individual units, appear to be compositionally related as shown by data and graphs. Sample locations are given in Appendix I.

Basalt-Andesites

Samples were collected from most flow units on the volcano's flanks, including samples SP-1, SSP-F, B8-5, and DG-2 to the northwest, CH-B to the northeast, and SU-F to the south. Samples NS-1, LC-1, LCF-F, LR-1, LP-F, TV-F, and MB-1 are from flows along the northwest fissure. Samples LB-1 thru LB-5 were donated by W. P. Leeman for trace element

analysis. These samples are all hypersthene- or augite-bearing basaltic andesites. Phenocrysts of plagioclase are numerous and of varying sizes up to several millimeters. Most of the larger plagioclase phenocrysts have a very moth-eaten texture. Few large pyroxene phenocrysts are present but many smaller ones are present in the ground mass. Magnetite is present in all samples to varying degrees and some apatite is present. Most samples collected, including flow samples, are filled with large vesicles indicating much gas in the magma as would be expected in the cinder cones. Samples FU-B, PI-B, PPCC-1, and CH-B were collected from cinder cones north of the caldera, EPP-2 from east of the caldera, and RE-B, DH-B, and FI-B from south of the caldera. The petrology of these scoria samples is similar to that of samples of lava flows. Inside the crater, RS and F-1 are from cinder cones on the north wall while ILB and B10-1 are from basaltic flows on the crater floor. These samples are also similar to the samples from the flows on the flanks of the volcano.

High-Iron Basalts

Sample DG-1 is from a flow northwest of the caldera and sample F-2 is from a cinder cone on the north wall of the caldera. Samples NPP-1 through NPP-3 and A2-3 are from flows in the walls of the caldera. All are similar to flows on the

flanks of the volcano with the exception of having fewer phenocrysts and larger amounts of magnetite.

Amota Butte Series

The Amota Butte rocks are described by Williams as hypersthene-bearing andesitic basalts and contain large moth-eaten plagioclase phenocrysts. The samples are older than other Newberry samples discussed.

Rhyolites

Samples MC2-A, MC2-B, EAB-1, EAB-3, CH-1, and CH-3 are from rhyolite domes west and east of the caldera while R8-2 is from a dome on the caldera floor. ILO and BOF are from obsidian flows on the caldera floor. R8-3 represents the oldest exposed unit at Newberry Crater, coming from the lower northeast wall of the caldera. PP-4 through PP-9 are from South Paulina Peak. These rhyolites showed large variations in coloring and textures and exhibited a great deal of banding. BOF and ILO are the only glassy samples. Small plagioclase laths are abundant in all other samples.

Newberry Area Samples

Several samples of rocks from the area, which are not a part of the Newberry suite, were analyzed in an effort to obtain some control on regional compositional variations and to show that the Newberry rocks are distinctive in a

compositional sense. The analyses of these rocks are reported along with those of the Newberry suite in Table 3f and are plotted on the variation diagrams as crosses (except for FS-B). They will not be treated in the discussion of magma differentiation which follows.

Two Newberry samples, FS-B collected east of the caldera and PF-1 from near Paulina Falls, are included in this group of samples. FS-B is similar to the basalt andesites but contains abundant olivine. PF-1 contains many clasts foreign to the tuffaceous ground mass.

The samples from Black Rock Butte and the McKenzie Pass area can not be compositionally separated from the Newberry samples except for slightly lower abundances of most of the trace elements. This observation suggests that aspects of the discussion of magma differentiation that follows might apply to suites of rocks from the nearby Cascades. These High Cascade rocks are olivine- and hypersthene-bearing basalts and andesites with abundant phenocrysts of plagioclase.

Three samples from the Pine Mountain area are different from the Newberry rocks in terms of trends and the models that will be discussed. These rocks contain many laths and small phenocrysts of plagioclase with small amounts of hypersthene.

Observations

Frequency distribution diagrams for SiO_2, Na_2O, and FeO are plotted in Figure 5. These diagrams represent only chemical compositions and in no way represent the relative volumes of rocks or groups of rocks at Newberry Crater.

The silica concentrations of the rocks show a remarkable bimodal distribution (excluding the older Amota Butte series) with a large gap. The basalt-andesite samples range from 48 to 58% SiO_2 while the rhyolites range from 71 to 75% silica. The Amota Butte series has silica contents lying between 63 and 66%, intermediate between the basalt-andesite and rhyolite silica values. That rocks from Newberry Crater have a discontinuous distribution of silica contents is a well known fact.

It is noteworthy that among the major element oxides, only sodium (see Figure 5) and aluminum do not exhibit a pronounced bimodal relationship. Although the basalt-andesite and rhyolite data tend to be different over-all, the range of sodium and aluminum abundances is nearly continuous and no concentration of samples around a particular value is observable for those two elements.

Iron contents are easily divided into four groups on the basis of concentrations around a particular value on the variation diagrams. Rhyolites contain from 1.5 to 3.5% iron; the Amota Butte series contains 5 to 6.5% iron; the basalt-

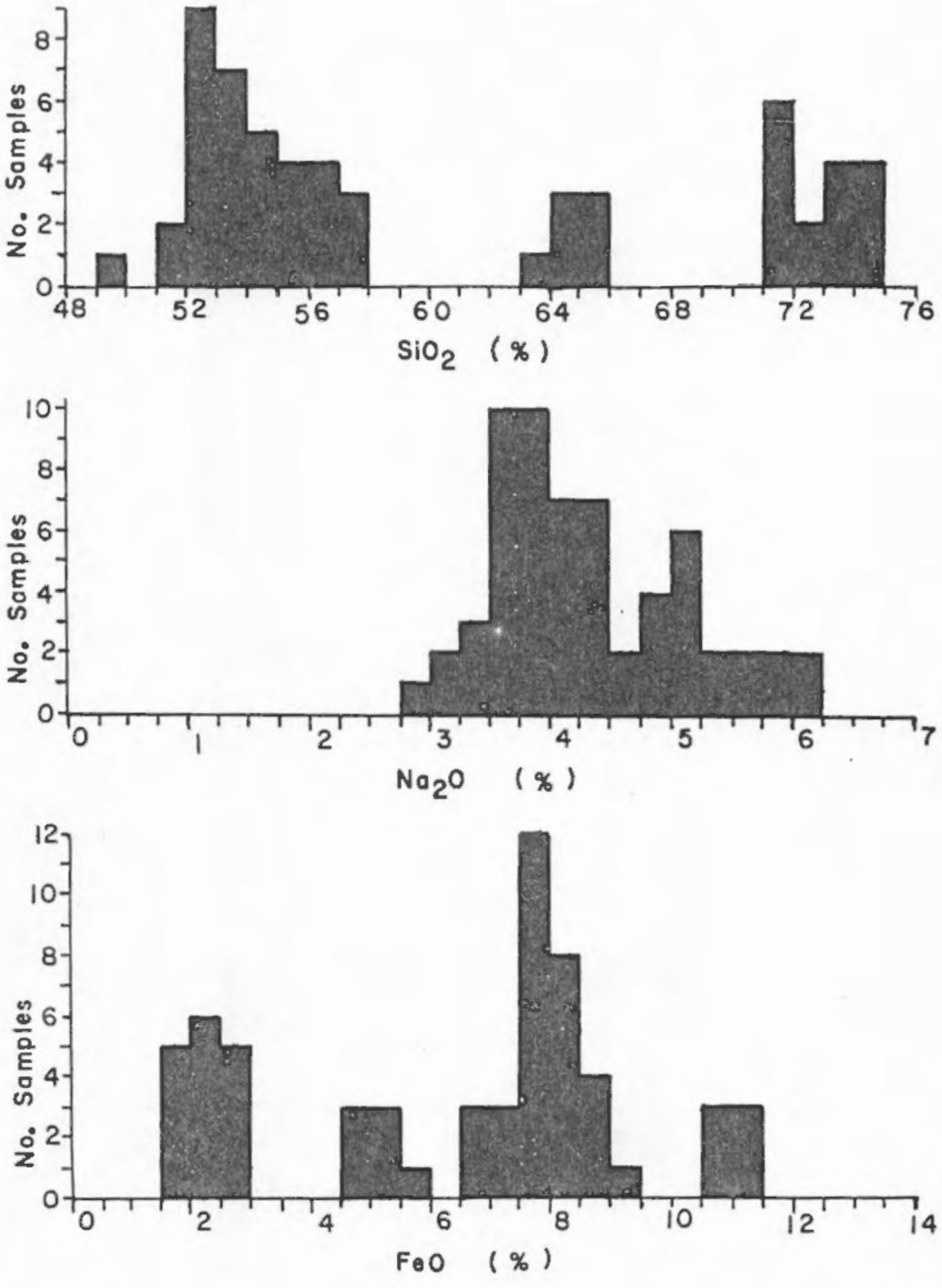

Figure 5. Frequency Distributions for SiO_2, Na_2O, and FeO.

andesite group from 7 to 10.5% iron; and the fourth group from 11.5 to 13% iron. The fourth group is also distinct in abundances of titanium and manganese, but tends to be in the basalt-andesite group for all other elements examined. The six samples making up this group are of pre-collapse age and older than the basalt-andesite group and most of the rhyolites.

A characteristic which is apparent upon study of the variation diagrams is the linear relationships between compositions of the basalt-andesite group and of the Amota Butte series. While in some cases the scatter of the basalt-andesite compositions is rather large and a straight line drawn would be of questionable validity, none of the variation diagrams exhibit a definite curved line between the groups. It is also apparent that the rhyolite values do not fall on this line.

A plot of logarithms of chondrite-normalized rare earth element abundances versus ionic radii for a typical basalt and a typical rhyolite are shown in Figure 6. The rhyolite is enriched over the basalt in all analyzed elements by a factor of about two except for europium which is depleted by a factor of about two. The depletion of europium is generally attributed to the crystallization of plagioclase in at least one stage of the rock's formation. The rare earth elements in general exhibit a normal continental pattern with enrichment of the light rare earth elements.

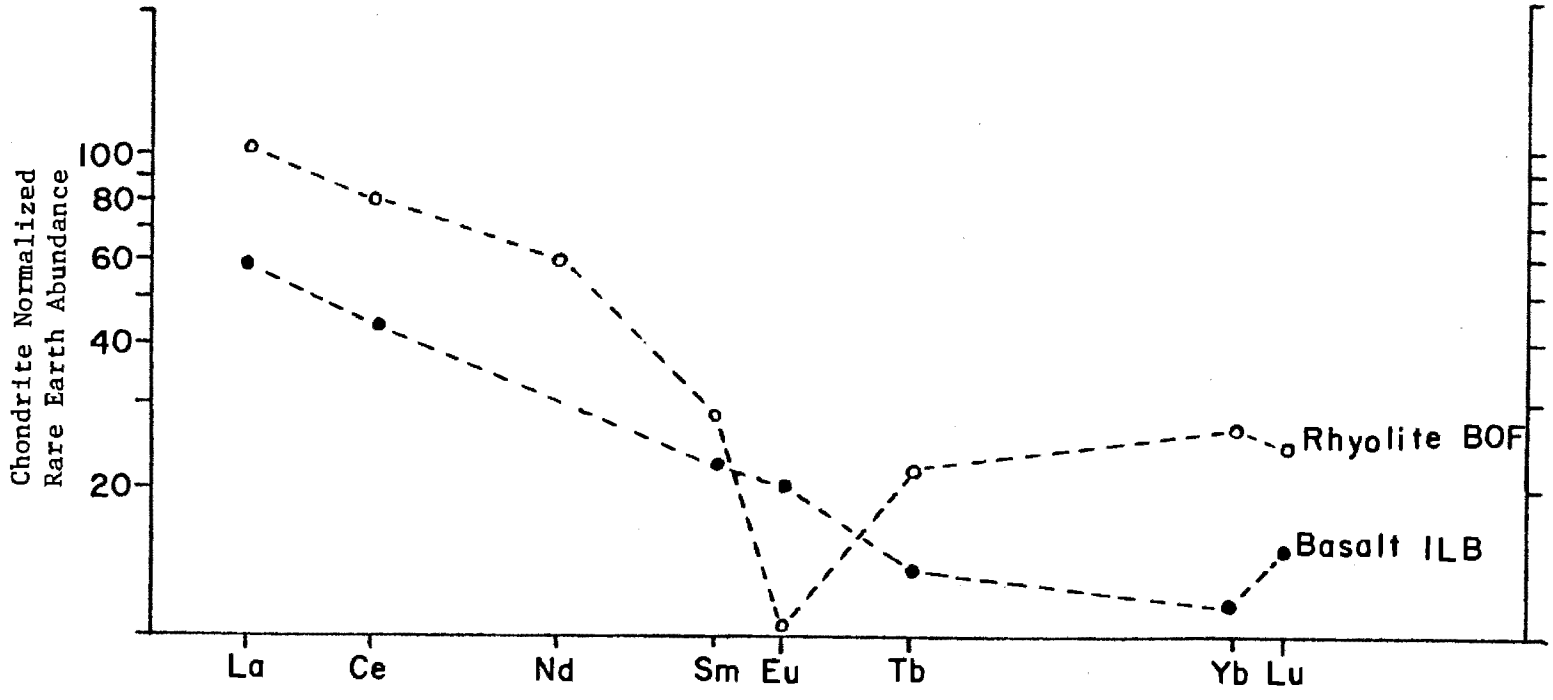

Figure 6. Rare Earth Element Plots for a Basalt and a Rhyolite from the Newberry Suite.

DIFFERENTIATION OF MAGMAS

Differentiation of a magma is the changing of the magma in some way so as to produce a compositionally different type of rock when it is cooled or to produce a family of rocks which can be described essentially by changing of magma compositional characteristics. There are several recognized processes for differentiation of a magma, but most of these are little understood. Knowledge of these processes is hampered by the fact that only the final product is observed in most cases and that erosion usually has not progressed to the point where other products of differentiation emplaced as intrusive bodies or left behind as residues are observable. Six differentiation processes are generally recognized. Others can be classified within these six general processes.

Crystal fractionation as applied to a differentiating magma is a process where a mineral or minerals crystalize in the cooling magma and are then separated from the liquid by some means, thereby changing the bulk composition of the magma that will form the observable end product. Gravity separation may occur with crystals that are more dense than the magma sinking and those which are lighter than the magma floating, or crystals may be filtered out of the magma if they aggregate to form a clot or felty mass and only the liquid is driven away from the site of crystal fractionation.

As the process of fractional crystallization proceeds, the elements enriched in the minerals being formed are depleted from the magma, and elements excluded from the minerals being formed are enriched in the magma because its volume is decreasing. Geochemists have studied trace element concentrations in many rocks and are beginning to understand how trace elements should behave in cases involving fractional crystallization.

Mixing of magmas is a process of magma differentiation which is not frequently substantiated from geological field evidence. It involves two magma types and their mixing to form the magma which produces the observable rock. The history of the resultant magma and therefore its differentiation path are complex and difficult to study. Mixing of magmas could easily be studied by means of simple mixing models if the composition of one of the original magmas were known along with that of the observable end product. However, the compositions of the magmas are usually unknown and any model of magma differentiation based on mixing of magmas can not be dealt with without knowledge of specific magma compositions.

Immiscibility of magmas involves the separation of one magma into two different and separate magmas, or the unmixing of magmas. Bowen reached the conclusion that "On the basis of immiscibility, it is impossible to build up an adequate explanation of the associated members of rock series

which is the fundamental problem of petrology." Experiments have shown that certain chemical compositions would yield immiscible liquids under reasonable pressure and temperature conditions and Roedder and Weiblen (1971) have demonstrated liquid-liquid immiscibility in lunar basalts and a few terrestrial rocks. Many petrologists have not ruled out immiscibility as a means of magma differentiation. The study of immiscibility would be subject to the same restraints as the mixing of magmas as well as knowledge of the distribution of elements into the two magmas under magmatic conditions.

Assimilation is a process in which the magma dissolves some of the wall rock which confines it. In its simplest sense, assimilation would only be the mixing of the magma with the dissolved wall rock. However, in a practical sense, equilibrium reactions occur between the wall rocks and the magma with or without any solution of the wall rock so that the differences in chemical potential for the elements involved are minimized. Various elements are exchanged at different rates. These exchanges cannot yet be described rigorously enough to be modeled systematically in natural systems. Assimilation occurring in the upper crust will alter the Sr^{87}/Sr^{86} isotope ratio, but this effect will only give evidence of assimilation in some parts of the crust and says nothing about what may occur below that level.

Volatile transfer is an ambiguous type of differentiation process involving volatile complexing and transfer of chemical elements. The chemical potential of volatile components and their complexes will vary with temperature and pressure, and therefore with depth, and any element in complexes will be transported within the body of magma as the complex seeks its equilibrium within the magma. Oxidized and reduced compounds of hydrogen, carbon, sulfur, and the halogens are probably the main complexing agents within the magma. As a magma is rising from its place of formation, it reaches a pressure at which it may no longer be able to contain its dissolved volatile components. At this stage, bubbles may be formed as a separate phase and rise, thereby transporting some elements to the upper parts of the rising magma. Two very different types of complexes are involved because of the liquid and gaseous phases and insufficient information is available to be able to study volatile transfer in this sense as a differentiation process.

Partial melting is a process of magma formation which may have a great deal to do with differentiation. It involves the melting of pre-existing rocks and is usually thought of as an upper mantle process. In this process, a change in a variable such as temperature, pressure, or content of volatile components will start a phase or phases within the source rock region to melt. If newly formed liquid is removed as the melting process continues, a magma

composition different from that of the original whole rock will be formed. (In the unlikely case of the liquid not being removed and the whole rock is melted, no differentiation would occur by means of such melting.) The question of attainment of equilibrium is also involved in that element transport across phase boundaries may occur and the chemical composition of the magma may thereby be changed. Partial melting may involve all of the types of magmatic differentiation mentioned here in some way or other. It can not be handled in detail by itself because the components of the rocks where it occurs are generally unknown. Partial melting may be discussed in the unrealistic sense that it is the opposite of fractional crystallization thereby yielding some insight into its possible effects from that way of thinking about it.

In a realistic sense, it is improbable that one and only one of these ways of magma differentiation can account for the observed compositions of rocks. Although one may start with a single model in explaining observed rocks, it is unrealistic to jump to any conclusion that we understand exactly how a magma was differentiated and that we can account for the process by which an observed rock was formed on the basis of that model.

A closer look at several differentiation processes will be taken with applications made to the basalt-rhyolite problem at Newberry Crater.

IMPLIED MAGMA DIFFERENTIATION PROCESSES AT NEWBERRY CRATER

Mixing

A study of the variation diagrams presented with the data in Figures 3a through 3d demonstrates that there is a nearly linear relationship between compositions of the basalt-andesite and the Amota Butte series of rocks and hence one infers an important characteristic of the Amota Butte rocks. The fact that all major, minor, and trace elements follow this trend is an indication that mixing of magmas is a major type of differentiation involved at Newberry Crater, but unmixing, or immiscibility, cannot be completely discounted in examining only the linear relationships shown by the variation diagrams.

There is no way to determine the concentrations of the individual elements in the two end members that would be involved, but they must lie on the line that could be drawn between the two rock groups for each element and possibly near (but at or beyond of course) the extremes of the elemental abundances found in the rocks involved. On the basis of the variation diagrams, no estimate of silica content can be made for the low-silica magma and only on the basis of the chromium variation can the high-silica magma be described because the chromium values for these samples approach zero

in rocks with silica contents near 65%. Herein the Amota Butte rocks take their importance: Their analyses possibly represent the composition of a magma involved in mixing to differentiate the basalt-andesite rocks of the Newberry Suite.

It must be re-emphasized that no one model can be used to describe rock differentiation. The scatter along the mixing line, particularly as shown by the aluminum variation diagram (see Figure 3a) could indicate that other processes of differentiation are involved in the formation of the basalt-andesite Newberry series of rocks.

Volatile Transfer

The numerous vesicles found in lava samples along with the large number of cinder cones and the pumice fall indicate that volatiles were plentiful in some of these magmas at the time of their eruptions. There is, at this time, no way to tell what part volatiles played in magma differentiation at Newberry Crater. However in the basalt-andesite group of rocks with prominent vesicles and cinders, mixing seems to be the predominant type of magma differentiation and volatile transfer would seem to be limited to minor differentiation in the rising magma, at best.

Fractional Crystallization

Fractional crystallization is generally accepted by geochemists as a means of magma differentiation. Bowen (1928) suggested that rhyolites were formed from basaltic parent magmas through the process of fractional crystallization. In his paper dealing with Newberry Caldera, Williams (1935) accepted this hypothesis but offered no direct evidence either for or against it. More recently, fractional crystallization has been questioned as a solution to the basalt-rhyolite problem. If it were important, rocks of intermediate silica contents (intermediate differentiates) would be expected in sufficient numbers to form a smooth distribution curve with the basalts and rhyolites. However, as is the case at Newberry Caldera, these intermediate rocks generally are missing in basalt-rhyolite complexes. Fractional crystallization generally starts with magmas having a basaltic composition and proceeds to more silicic compositions suggesting that basalts would be erupted first, followed by more silicic rocks as time progresses. At Newberry Crater, the suggested trend is not followed. Three age groups of rhyolites are found and basaltic magmas were erupted between the times of rhyolite eruption.

Despite the improbability of magma differentiation by fractional crystallization at Newberry Crater, it seems worthwhile to apply our knowledge of this type of

differentiation to the major and trace element data to see if any information can be brought to light regarding this process and the basalt-rhyolite problem. The boundary conditions I have applied in my approach are extremely liberal in hopes of obtaining some type of a fit for fractional crystallization models. Mixing models using analyzed rocks and stoichiometric major element compositions of minerals were used to determine amounts of minerals crystallized for a given magma transition. High and low values selected from published trace element distribution coefficients for the minerals involved (see Table 2) were then applied to trace element data for a parent magma, assumed to be represented by an analyzed rock, to determine if the abundances of those elements in the resulting magma, represented by another analyzed rock, could be accounted for by the process of fractional crystallization.

If crystal fractionation were the major cause of magma differentiation at Newberry Crater, there should be little trouble in reproducing the composition of any rock sample analyzed from another appropriate sample by models of this kind.

Distribution Coefficients

Crystals form spontaneously in the magma when the proper conditions are allowed by the variables involved.

Table 2. Selected Partition Coefficients From the Literature.

ELEMENT	PLAGIOCLASE	CLINOPYROXENE	ORTHOPYROXENE	OLIVINE
Co	0.055[5] -0.51[5]	1.1[1] - 22.2[2]	2.1[1] -47.9[2]	3.[1]
Cr	0.06[5] -0.67[5]	18.[1] ->200.[6]	0.2[1] -35.4[2]	1.2[1]
Sc	0.018[2] -0.197[5]	2.9[1] - 32.9[2]	1.2[1] - 8.7[2]	0.5[1]
Ba	0.0537[3]-1.43[1]	0.02[6] - 0.388[3]	0.01[6] - 0.06[6]	--
Rb	0.007[6] -0.46[3]	0.0129[3] - 0.284[3]	0.0148[3] - 0.0287[3]	--
K*	0.0188[3]-1.60[5]	0.0185[3] - 0.273[3]	0.00908[3]- 0.0190[3]	--
La	0.09[1] -0.49[5]	0.08[1] - 0.33[2]	0.064[2] - 0.1[4]	0.0026[1]
Sm	0.024[3] -0.168[5]	0.38[4] - 2.15[2]	0.047[3] - 0.43[2]	0.0027[1]
Eu	0.055[3] -4.2[5]	0.39[4] - 1.40[2]	0.079[3] - 0.33[2]	0.0046[1]
Lu	0.02[1] -0.24[3]	0.9[1] - 2.2[2]	0.11[1] - 0.82[2]	0.0139[1]
Hf	0.04[1] -0.17[5]	0.6[1]	--	0.01[1]

*Although potassium is a major rock forming element, it is not a major component for any of the minerals used and is therefore concentrated in the liquid during crystallization of the above minerals.

[1]Corliss (1970).

[2]Radke, unpublished results from Crater Lake, Oregon.

[3]Schnetzler and Philpotts (1970) and Philpotts and Schnetzler (1970).

[4]Schnetzler and Philpotts (1968).

[5]Dudas et al. (1971).

[6]Ewart and Taylor (1969).

The process is slow and small changes in the variables in the opposite direction may result in the redissolving of the crystals by the magma. In this situation, the conditions at the surface of the growing crystal approach equilibrium. Assuming equilibrium conditions, the chemical potentials for any given component in the portion of the two phases which are in equilibrium must be equal.

$$\mu_{il} = \mu_{im} \tag{1}$$

where μ represents the chemical potential of the component i, l for the liquid, and m for the mineral phase. Under conditions other than ideal, which would in general include magmatic conditions,

$$\mu_{il}^{*} + RT \ln a_{il} = \mu_{im}^{*} + RT \ln a_{im} \tag{2}$$

where μ^{*} represents the standard chemical potential, R is the gas-law constant, T is the temperature and a represents the activity of the component under consideration. Rearranging,

$$\ln \frac{a_{im}}{a_{il}} = \frac{\mu_{il}^{*} - \mu_{im}^{*}}{RT} \tag{3}$$

The distribution coefficient can now be defined in terms of the activities of the components,

$$D = \frac{a_{im}}{a_{il}} \tag{4}$$

where D represents the distribution coefficient. From equation 3, the only variable other than the activities to which the distribution coefficient is related is temperature.

Activities of trace elements are, at best, difficult or impossible to measure in our present state of technology. However, for very small concentrations of a trace element in a magma, we may assume that the concentration of that trace element approximates its activity in the magma. Concentrations of trace elements in rocks can be determined and most of the known distribution coefficients are approximations based on concentrations.

$$D_c = \frac{c_{im}}{c_{il}} \qquad (5)$$

where D_c represents the distribution coefficient determined by the concentrations, and c is the concentration of component i in the liquid or solid.

Distribution coefficients may be applied by use of the Rayleigh Distribution Law which is represented by the equation

$$\frac{c_2}{c_1} = F^{(D_c - 1)} \qquad (6)$$

where c_1 represents the concentration of the trace element in the starting magma, c_2 represents the concentration in the liquid after crystals have been removed, F is the fraction of liquid remaining after crystallization, and D_c is

the distribution coefficient for the element under consideration between the liquid and the crystal. The Rayleigh Distribution Law is valid under the condition where the liquid is in equilibrium with the skin or outside portion of the forming crystal, a condition similar to that found in many natural systems. At Newberry Crater the large number of vesicles in some samples and the pumice fall indicate the magma did not remain in a shallow chamber for a sufficient time to de-gas and therefore not long enough for any crystals to equilibrate with the magma. The Rayleigh Distribution Law would be especially applicable for this case.

This equation can be applied for only one mineral phase at a time. If two or more minerals crystallize from the magma, the order in which they crystallize is important since results of calculations to predict trace element concentrations differ, sometimes substantially, if the order of crystallization of minerals is altered. Therefore some knowledge of the order and relative rates of crystallization is important in any fractional crystallization scheme. In order to handle part of this problem, M. M. Lindstrom and D. J. Lindstrom (personal communication) developed an equation which takes into account the simultaneous crystallization of several minerals. It may be expressed as

$$\ln \frac{C_2}{C_1} = \frac{\ln F}{\Sigma j_i} \Sigma[j_i(D_{ci}-1)] \qquad (7)$$

where c_1, c_2, F, and D_c are the same as in equation 6 and j represents the fraction of mineral i crystallized.

Distribution coefficients have been published which have been determined on the basis of concentrations of trace elements in minerals and ground mass. To determine values of distribution coefficients, minerals must be known to be in equilibrium with the co-existing magma. If the crystal shows any zoning or is rimmed, it is definitely not in equilibrium with the liquid and can not be used in a simple way for the determination of distribution coefficients. The history of the crystal and its immediate surroundings can usually be established in at least a crude way by the study of thin-sections with a microscope.

The problem of analysis of the mineral and its purity is important. There are few technical systems known today which can analyze minerals for a variety of trace elements with concentrations in the parts-per-million (ppm) range without separation of the mineral of interest from coexisting glass or groundmass. Minerals can be separated from glass or groundmass, but the small bits of contaminants clinging to the crystal are critical. For example in an extreme case, if a small crystal of olivine with a sodium concentration of around ten ppm has clinging to it a small piece of groundmass with a sodium concentration of around two percent (20,000 ppm), the sodium analysis of the "olivine" would be of no scientific value.

Distribution coefficients have been determined experimentally (Drake, 1972 and D. J. Lindstrom, personal communication) in doped systems where the concentration of the trace element of interest is increased to the point where it can be detected by analytical means without mineral separations. These determinations are generally in agreement with determinations made from natural systems.

Selected partition coefficient data, comprising reasonable ranges of high and low values from the literature, are given in Table 2. As shown in equation 3, the distribution coefficients vary with temperature. A variety of rocks and rock systems with different thermal histories were used for determinations of the distribution coefficients, so that the range observed reflects these variables.

Distribution coefficients are associated with minerals on the basis of their crystal structure, not on the basis of the major elements which form the mineral. At present, no distinction is made between iron- or magnesium-rich olivines in the application of distribution coefficients. Likewise in applying distribution coefficients to pyroxenes, no distinction is made on the basis of iron, magnesium, or calcium concentrations (although ortho-pyroxenes have limited calcium contents because of their large ionic radius), but it makes a great deal of difference whether the pyroxene is in the orthorhombic or monoclinic crystal habit. Plagioclases, of the continuous series, may be described in terms of variations

in sodium and calcium contents and are not distinguished in considering distributions of trace elements, although in some circumstances other crystal habits occur which are given different names and must have their own distribution coefficients applied. Changes in composition along one of these solid-solution series are generally reflected in changes in equilibration temperatures and so, indirectly, affect distribution coefficients.

The different crystal habits will allow for various trace element impurities depending on the ionic radii, crystal imperfections, lattice configuration, charge on the ion involved, and ability to fit into the crystal field of the mineral. For one reason or another, some trace element ions are rejected by all the minerals that are involved in the early stages of fractional crystallization of a cooling magma. These elements are enriched in the final magma because of its decreasing volume.

Crystallizing minerals that leave the scene of crystallization and are effectively separated from the magma cannot stay in equilibrium with the magma as it evolves and must be compared, for model-building purposes, with the magma composition in which they were formed. In many cases, this magma no longer exists and consequently its characteristics must be inferred. Crystals which are resorbed by a magma would enrich the magma in those trace elements initially present in notable abundance in the crystals, thereby causing

changes in the trace element equilibrium concentrations in newly forming minerals. These problems are certainly in part reflected in the published partition coefficient data and would be involved in some way in models applied to natural systems. Consequently, one would not expect to find exact agreement between calculated and observed abundances in such models.

Fractional Crystallization at Newberry Crater

Williams (1935) and Higgins (1973) describe mineral compositions found in rocks at Newberry Crater. They found that plagioclase is the predominant mineral formed during magma crystallization. Other minerals found in significant abundances in various rocks are olivine, orthopyroxene, clinopyroxene, and magnetite. Minor amounts of alkali feldspar, apatite, and some amphiboles are also found.

I explored paths of magma differentiation by allowing one rock analysis or an average of several analyses to represent a "parent magma" composition and another rock analysis to represent the final product of differentiation by fractional crystallization. Stoichoimetric proportions of the major element oxides as well as approximated compositions of significant rock forming minerals found in Newberry rocks are listed in Table 3.

Table 3. Composition of Minerals Used in Mixing Models.

	COMPOSITION	SiO_2	Al_2O_3	FeO	MgO	CaO	Na_2O
	Olivine						
*	Fe_2SiO_4	29.49	--	70.51	--	--	--
*	Mg_2SiO_4	42.70	--	--	57.30	--	--
1	$Fe_{20}Mg_{80}$	40.06	--	14.10	45.84	--	--
	Pyroxenes						
*	$FeSiO_3$	45.54	--	56.46	--	--	--
*	$MgSiO_3$	59.85	--	--	40.15	--	--
*	$CaSiO_3$	51.73	--	--	--	48.27	--
	Orthopyroxenes						
2	$Ca_7Mg_{61}Fe_{22}$	54.70	--	17.43	24.49	3.38	--
3	$Ca_4Mg_{97}Fe_{19}$	56.80	--	10.35	30.92	1.93	--
4	$Mg_{35}Fe_{65}$	50.55	--	35.40	14.05	--	--
5	$Mg_{60}Fe_{40}$	54.13	--	21.78	24.09	--	--
6	$Mg_{65}Fe_{35}$	54.84	--	19.06	26.10	--	--
7	$Mg_{70}Fe_{30}$	55.56	--	16.34	28.11	--	--
	Clinopyroxenes						
8	$Ca_{30}Mg_{30}Fe_{40}$	51.69	--	21.78	12.05	14.48	--
9	$Ca_{45}Mg_{45}Fe_{10}$	54.75	--	5.46	18.07	21.72	--
10	$Ca_{50}Mg_{50}$	55.79	--	--	20.07	24.14	--
	Plagioclase						
*	$CaAl_2Si_2O_8$	43.16	36.65	--	--	20.16	--
*	$NaAlSi_3O_8$	68.74	19.44	--	--	--	11.82
11	$Ca_{30}Na_{70}$	61.08	24.60	--	--	6.05	8.27
12	$Ca_{40}Na_{60}$	58.53	26.32	--	--	8.06	7.09
13	$Ca_{50}Na_{50}$	55.97	28.04	--	--	10.08	5.91
14	$Ca_{60}Na_{40}$	53.41	29.77	--	--	12.11	4.73
15	$Ca_{70}Na_{30}$	50.85	31.49	--	--	14.1	3.55
	Magnetite						
16*	Fe_3O_4	--	--	93.09	--	--	--

* End-member containing only one cation.

+ Numbers correspond to compositions in Table 5.

In order to test any model involving fractional crystallization as a magma differentiation process, specific samples had to be chosen to represent concentrations of beginning and final magmas. The analyses of these samples are given in Table 4. For mixing model purposes, several groupings were used and the average analyses representing these groupings are also given in Table 4. These groupings are shown by circles on the variation diagrams presented with the analytical data in Figures 3a through 3d.

Pre-Bas represents a group of iron enriched "pre-collapse" basalts found in the rim of the caldera and on the slopes. Higgins (1973) believes the composition differences between the iron enriched basalts and the basalt-andesites are due mainly to contrasts in the oxygen fugacity before and after formation of the caldera.

AM-Avg represents an average of the seven Amota Butte rocks. These are "pre-Newberry" rocks, certainly older than the other samples collected. However, being located within a reasonable distance of Newberry Crater, their composition may tell something about the chemical system which is responsible for Newberry rocks. If these rocks are related to Newberry Crater samples, and they fit nicely as shown in Figures 3a through 3d, it is quite possible that similar compositions of magmas or rocks might be involved at Newberry Crater. Samples AM-2 and AM-6 were used in models along with AM-Avg so the extremes of the group were also studied.

Table 4. Analyses and Averages Used in Mixing Models.

Sample Name	FS-B	RS	Pre-Bas[1]	B8-5	Pri-Mag[2]	LC-1	LP-F	B10-1	FI-B	AM-6	AM-Avg[3]	AM-2	PP-Avg[4]	BOF	CH3	EAB-1
Major elements as oxides (%)																
SiO_2	48.8	51.8	52.4	52.9	53.3	54.8	55.6	55.8	57.6	63.0	64.7	65.7	71.4	73.2	73.6	74.9
TiO_2	1.03	1.27	2.26	0.93	1.28	1.21	0.99	1.53	1.02	0.93	0.85	0.82	0.33	0.26	0.20	0.16
Al_2O_3	17.6	17.7	15.4	19.1	17.1	16.6	17.3	16.1	16.9	16.6	16.2	15.9	14.6	14.0	13.7	13.8
FeO*	9.09	7.60	11.03	6.87	8.07	7.78	6.51	8.52	6.75	5.64	5.12	4.77	2.70	2.02	2.32	1.55
MnO	0.17	0.14	0.20	0.13	0.16	0.16	0.14	0.16	0.14	0.15	0.15	0.12	0.11	0.06	0.07	0.02
MgO	8.06	6.19	3.91	5.77	5.28	5.02	5.07	*3.67	4.14	1.51	1.15	0.98	0.41	0.23	0.23	0.33
CaO	10.80	9.68	7.94	9.66	8.97	8.37	8.13	7.29	6.91	4.12	3.40	2.87	1.16	0.88	0.79	0.80
Na_2O**	2.90	3.36	4.29	3.12	3.63	3.84	3.69	4.19	4.18	4.86	5.13	5.43	5.93	5.07	5.02	4.20
K_2O	0.36	0.97	0.91	0.58	0.98	1.13	1.52	1.43	1.39	2.28	2.52	2.57	3.03	4.08	3.80	4.06
P_2O_5	0.25	0.43	0.44	0.18	0.31	0.25	0.29	0.40	0.24	0.27	0.25	0.25	0.04	0.02	0.01	0.02
Minor and trace elements (ppm except as noted)																
Na (%)	2.15	2.45	3.16	2.31	2.85	2.84	2.71	3.14	3.08	3.56	3.77	4.03	4.39	3.73	3.72	3.11
Rb	—	--	--	—	—	—	--	--	--	45.	59.(4)	--	71.	113.	105.	120.
Cs	--	--	--	—	--	0.9	1.0	1.0	1.3	1.9	1.7(5)	--	2.1	4.2	2.8	4.2
Ba	—	530.	360.	300.	390.	330.	610.	410.	640.	870.	920.	950.	950.	980.	1050.	1090.
La	7.	21.	15.	8.	15.	13.	21.	20.	16.	22.	24.	24.	28.	31.	30.	27.
Ce	14.	45.	30.	18.	30.	27.	41.	40.	28.	41.	43.	42.	53.(4)	—	53.	--
Nd	--	--	--	--	26.(3)	25.	--	23.	--	--	31.(3)	35.	36.	35.	39.	30.
Sm	3.2	6.0	6.8	3.2	4.9	4.8	5.9	6.5	5.2	7.2	7.4	8.0	7.6	6.7	8.6	5.2
Eu	1.12	1.75	2.18	1.05	1.55	1.42	1.57	1.88	1.73	1.86	1.91	1.82	1.52	0.92	1.27	0.83
Tb	0.5	0.6	1.0	0.4	0.7	0.7	0.7	0.8	0.8	1.1	1.1	1.2	1.2	1.2	1.4	0.8
Yb	2.3	1.6	3.6	1.4	2.4	2.4	2.4	3.0	3.9	3.3	3.9	3.7	5.3	4.7	5.1	3.2
Lu	0.42	0.31	0.58	0.26	0.39	0.42	0.43	0.44	0.48	0.58	0.67	0.70	0.79	0.76	0.90	0.45
Th	0.7	2.7	1.5	0.9	2.2	2.8	4.4	2.3	3.3	6.9	6.3	5.4	7.6	13.9	11.8	14.0
Zr	--	--	--	--	--	--	--	--	--	170.	180.(2)	--	300.	230.	260.	190.
Hf	1.8	3.1	4.1	2.0	3.2	3.2	4.1	4.5	4.1	4.8	5.4	5.8	8.4	9.0	8.0	6.0
Ta	0.9	0.4	0.7	0.3	0.5	0.6	0.6	0.7	0.5	0.7	0.6(4)	--	1.1	1.5	0.8	0.8
Fe (%)	6.81	5.92	8.45	5.53	6.26	6.07	4.90	6.61	5.16	4.33	3.93	3.68	2.05	1.57	1.77	1.15
Co	43.4	31.1	31.0	31.2	30.1	29.0	24.9	24.0	21.8	8.9	6.5	4.1	0.8	0.9	0.8	0.4
Sc	34.8	27.1	35.3	24.7	29.7	29.0	22.9	28.0	22.0	16.6	15.1	14.4	9.21	6.36	9.91	4.47
Cr	118.	117.	--	133.	97.	107.	92.	26.	77.	—	5.(2)	--	3.(3)	--	--	1.

* Total Fe recalculated as FeO.
** Calculated from INAA Na data.
1 Average of six samples, see Table 1a.
2 Average of six samples, see Table 1c.
3 Average of seven samples, see Table 1d.
4 Average of five samples, see Table 1d.

PP-Avg is an average of the five Paulina Peak samples.

There is no evidence as to the actual composition of the starting magma, but some starting point is necessary in order to study the differentiation process by fractional crystallization. The composition chosen, Pri-Mag, is in the lower silica abundance range and is the average of six samples that fall in a close composition range for all elements analyzed. Other samples were excluded because all of their elemental abundances do not fall within the close range of the main group.

The initial magma composition, the product composition, and the various mineral compositions were mixed by a computer using a program developed by Bryan, et al. (1969) and adapted by A. R. Duncan. The quality of a particular mix was judged by examining the sum of the squares of the differences of the elements being compared and the sum of the squares of the percent differences in the mix. A mix with the lowest values of these indicators and for which the proportion of minerals used in mixing was in agreement with the observed minerals was regarded as the best mix for the rocks and minerals involved.

Results of Mineral Mixes

Two approaches were used in applying mixing models to the data from Newberry Crater. First, a selected primary magma type was used to try to reproduce each of the selected

final rock compositions, and second, a step sequence was used to model differentiation from the primary magma to more silicic final rock compositions. In the first case, it was almost impossible to subtract linear combinations of mineral compositions from the initial magma to produce a good final rock composition for cases with large silica variations, from basalts to rhyolites for example. Results of both approaches are intermixed in Table 5, ordered by increasing silica concentration in the final magma. Table 5 shows the samples used to represent the initial and final magmas (see Table 4 for analyses). The percentage of initial magma removed as minerals (see Table 3 for composition) to form the final magma is found under the headings of the minerals removed in the mix. The first four mixes represent accumulations of the minerals which are mixed with the initial magma to form the final magma.

Pre-Bas could only be reasonably formed from Pri-Mag if the average Amota Butte composition was included as a mixing component. To obtain a mathematically reasonable mix without the Amota Butte average composition, it was necessary to add magnetite while subtracting other mineral compositions. The composition of the plagioclase, An_{20}, in the best fit suggests that this average basalt could be related to the accumulation of minerals which might have been formed from a fractionating rhyolite magma and then somehow incorporated into the primary magma with some further

Table 5. Results of Mixing Model Processes.

INITIAL MAGMA	FINAL MAGMA	PLAGIOCLASE COMP.*	PLAGIOCLASE AMT.	CLINOPYROXENE COMP.*	CLINOPYROXENE AMT.	ORTHOPYROXENE COMP.*	ORTHOPYROXENE AMT.	OLIVINE COMP.*	OLIVINE AMT.	MAGNETITE COMP.*	MAGNETITE AMT.	OTHER COMP.	OTHER AMT.	INDICATORS** 1	INDICATORS** 2	
+ Pri-Mag	Pre-Bas	11	31%	8	16%	--	--	--	--	16	5%	Pri-Mag	39%			
												Am-Aug	7%	0.25	6.60	+
+ Pri-Mag	FS-B	15	28%	10	9%	--	--	1	8%	16	4%	Pri-Mag	52%	0.72	4.95	+
+ Pri-Mag	BB-5	15	29%	--	--	2	11%	--	--	--	--	Pri-Mag	59%	1.01	4.89	+
+ Pri-Mag	RS	14	25%	9	5%	5	7%	--	--	16	2%	Pri-Mag	60%	0.01	0.07	+
Pri-Mag	BIO-1	15	18%	10	5%	--	--	1	4%	16	8%	--	--	0.00	0.01	
Pri-Mag	PI-B	14	24%	9	9%	7	4%	--	--	16	3%	--	--	1.50	7.79	
Pri-Mag	LC-1	14	16%	9	4%	6	3%	--	--	16	2%	--	--	0.00	0.01	
Pri-Mag	LP-F	13	20%	9	6%	7	2%	--	--	16	3%	--	--	0.00	0.11	
LC-1	LP-F	11	9%	9	5%	--	--	--	--	16	2%	--	--	0.14	0.64	
LP-F	AM-6	14	35%	9	10%	6	10%	--	--	16	2%	--	--	0.31	1.71	
Pri-Mag	AM-Avg	14	38%	9	14%	--	--	1	5%	16	5%	--	--	0.00	0.01	
LP-F	AM-Avg	14	38%	9	11%	6	11%	--	--	16	2%	--	--	0.00	0.02	
LP-F	AM-2	14	40%	9	11%	6	11%	--	--	16	2%	--	--	1.05	5.65	
AM-6	PP-Avg	14	24%	9	2%	4	6%	--	--	16	2%	--	--	0.74	2.85	
AM-Avg	PP-Avg	15	16%	9	1%	3	2%	--	--	16	3%	--	--	0.01	0.05	
AM-2	PP-Avg	14	15%	9	1%	6	2%	--	--	16	2%	--	--	0.16	0.68	
AM-6	BOF	13	29%	9	3%	6	3%	--	--	16	4%	--	--	1.78	10.74	
AM-Avg	BOF	14	29%	9	2%	4	4%	--	--	16	1%	--	--	0.00	0.03	
AM-2	BOF	11	29%	9	3%	4	3%	--	--	16	3%	--	--	0.14	12.99	
AM-6	CH-3	13	31%	9	3%	6	4%	--	--	16	4%	--	--	2.34	13.64	
AM-Avg	CH-3	12	31%	9	2%	4	5%	--	--	16	1%	--	--	0.01	0.08	
AM-2	CH-3	11	29%	9	2%	6	1%	--	--	16	3%	--	--	0.22	21.08	
AM-6	EAB-1	12	37%	9	3%	6	3%	--	--	16	4%	--	--	0.92	24.89	
AM-Avg	EAB-1	11	35%	9	4%	6	1%	--	--	16	4%	--	--	0.14	5.59	
AM-2	EAB-1	11	35%	9	3%	6	2%	--	--	16	4%	--	--	0.90	77.12	

* Numbers in this column correspond to mineral compositions in Table 3.

** Indicator 1 is the sum of the differences of the expected final magma and the calculated magma concentrations. Indicator 2 is the sum of the squares of those differences.

\+ No crystal fractionation for these transitions. The final magma is formed by mixing compositions of the minerals and other components.

fractionation. The amount of clinopyroxene involved in the mix is large and it has an extremely high iron content and does not fit into any pattern of crystal fractionation studied in terms of other mixing models. Thus, the model is petrologically implausible.

Samples FS-B, B8-5, and RS each have silica contents less than that of the primary magma and, in terms of the mixing model, are best described as containing accumulations of crystals fractionated elsewhere from the assumed primary magma. FS-B, from a flow several miles east of the caldera, could be related to B10-1 on the basis of olivine found necessary with those mixes. B8-5 and RS accumulations could be related to several of the other mixes used, but in no case very closely. Samples B10-1, LP-F, and FI-B best fit into the mixing model in terms of the primary magma losing crystals, possibly by gravity settling.

The Amota Butte average, AM-Avg could be formed satisfactorily by the mixing models, but the rhyolites could not be formed directly from the primary magma.

The step sequence started with the primary magma. The composition of sample LC-1 could satisfactorily be modeled by fractional crystallization, but the step from LC-1 to LP-F was hardly satisfactory in terms of the low-calcium plagioclase, An_{30}, which is not observed in the basalt-andesite group of rocks. The low anorthite content was also reflected in the primary magma to LP-F mix. The

steps were split into three parts and LP-F was used to duplicate the compositions of the Amota Butte series, AM-6 with the highest silica value of the series, AM-Avg averaging all compositions of the series, and AM-2 with the lowest silica value of the series. Each of the Amota Butte compositions could be duplicated.

These steps were studied on the basis of rock compositions involved at Newberry Crater and are not real in a practical sense in light of the differences in order of appearance of these rocks.

The three Amota Butte compositions were each used to form four rhyolites. The rhyolites could be successfully formed by the mixing model in terms of plagioclase, clinopyroxene, orthopyroxene, and magnetite although the sums of the squares of the percent differences are higher than accepted for other models. Late stages of extreme differentiation could involve minor minerals such as biotite, hornblende, sanidine, and apatite which appear in small amounts as minerals of the rocks involved.

Trace Element Fractionation

Percentages of minerals crystallizing in going from one magma composition to another are found in Table 5. These mineral compositions were used with high and low values of distribution coefficients as found in Table 2 to bracket the analyzed final composition used in the particular model.

The results are found in Tables 6a, 6b, and 6c. Where bracketing was not achieved, the last column indicates the percent of the actual concentration by which the mix failed, a plus sign indicating greater than the highest calculation, and a minus sign indicating lower than the lowest calculated concentration. Those transitions which were modeled as crystal accumulations from the primary magma were not tested owing to lack of sufficient constraints.

Cobalt final compositions can be bracketed for the basalt-andesite transitions. In the rhyolite transitions it is sometimes within the bracket and sometimes lower than the lower calculated composition indicating a greater loss of cobalt than fractional crystallization would predict and that the model removes too much pyroxene.

Chromium contents of the final magma are higher than the predicted values for the basalt-andesite transitions indicating that the model would remove too much chromium. Chromium is too low for detection in many of the rhyolites. One should note that appreciable chromium may have been removed in magnetite. If this loss is taken into account, the predicted values would then be even lower.

Scandium contents of the final magmas generally agree with those predicted but trends are similar to cobalt in some of the rhyolite transitions.

Barium is generally predicted and found to be concentrated in the magma but it behaves erratically in the

Table 6a. Trace Element Results Using Crystal Fractionation Processes.

TRACE ELEMENT	CONC. INITIAL MAGMA	CONCENTRATION PREDICTED HIGH	CONCENTRATION PREDICTED LOW	CONC. FINAL MAGMA	% FROM PREDICTED CONC.
Pri-Mag To B10-1					
18% Plag - 5% Cpx - 4% Oliv - 8% Mag					
Co	30.1	33.4	8.2	24.0	
Cr	97.1	41.6	<0.001	26.4	
Sc	29.7	32.1	4.9	28.0	
Ba	390.	511.	368.	412.	
Rb	20.	26.	24.	—	
K	0.81	1.07	0.75	1.11	+3.6%
La	15.2	20.7	18.3	20.1	
Sm	4.86	6.58	5.72	6.47	
Eu	1.55	2.08	0.78	1.88	
Lu	0.388	0.509	0.426	0.441	
Hf	3.21	4.42	4.29	4.52	+2.2%
Pri-Mag to F1-8					
24% Plag - 9% Cpx - 4% Opx - 3% Mag					
Co	30.1	37.6	0.28	21.8	
Cr	97.1	19.1	0.007	77.4	+75.%
Sc	29.7	31.9	0.7	22.2	
Ba	390.	614.	384.	638.	+3.8%
Rb	20.	32.	27.	12.	-125.%
K	0.81	1.29	0.77	1.56	+17.3%
La	15.2	23.4	19.0	16.1	+19.3%
Sm	4.86	7.39	5.66	5.21	-8.6%
Eu	1.55	2.33	0.57	1.73	
Lu	0.388	0.555	0.431	0.483	
Hf	3.21	4.80	4.61	4.07	-13.3%
Pri-Mag to LC-1					
16% Plag - 4% Cpx - 3% Opx - 2% Mag					
Co	30.1	34.3	2.4	29.0	
Cr	97.1	54.3	0.003	107.0	+49.%
Sc	29.7	32.4	6.1	29.6	
Ba	390.	503.	382.	325.	-17.5%
Rb	20.	26.	24.	—	
K	0.81	1.05	0.77	0.94	
La	15.2	19.4	17.3	13.2	-31.%
Sm	4.86	6.19	5.48	4.75	-15.4%
Eu	1.55	1.96	0.86	1.42	
Lu	0.39	0.48	0.425	0.42	-2.4%
Hf	3.21	4.00	3.91	3.17	-27.%
Pri-Mag to LP-F					
20% Plag - 6% Cpx - 2% Opx					
Co	30.1	36.4	2.4	24.9	
Cr	97.1	37.3	<0.001	91.9	+59.%
Sc	29.7	32.4	3.2	22.9	
Ba	390.	535.	399.	605.	+11.6%
Rb	20.	28.	24.	19.	-26.%
K	0.81	1.12	0.76	1.27	+11.8%
La	15.2	20.5	17.8	21.2	+3.3%
Sm	4.86	6.53	5.52	5.86	
Eu	1.55	2.02	0.72	1.57	
Lu	0.388	0.502	0.428	0.431	
Hf	3.21	4.30	4.11	4.10	-0.2%

TRACE ELEMENT	CONC. INITIAL MAGMA	CONCENTRATION PREDICTED HIGH	CONCENTRATION PREDICTED LOW	CONC FINAL MAGMA	% FROM PREDICTED CONC.
Pri-Mag to AM-Avg					
38% Plag - 14% Cpx - 5% Oliv - 5% Mag					
Co	30.1	44.1	0.3	6.5	
Cr	97.1	4.1	<0.001	4.8	+14.6%
Sc	29.7	33.8	0.04	15.1	
Ba	390.	849.	345.	920.	+7.7%
Rb	20.	46.	32.	59.	+22.%
K	0.81	1.80	0.78	2.09	+13.9%
La	15.2	34.5	24.2	23.6	-2.5%
Sm	4.86	10.73	6.69	7.37	
Eu	1.55	3.35	0.23	1.91	
Lu	0.388	0.766	0.506	0.671	
Hf	3.21	7.52	6.97	5.35	-30.%
LP-F to AM-Avg					
38% Plag - 11% Cpx - 11% Opx - 2% Mag					
Co	24.9	35.5	<0.001	6.5	
Cr	91.9	9.9	<0.001	4.8	
Sc	22.9	28.6	0.04	15.2	
Ba	605.	1490.	612.	920.	
Rb	19.	48.	35.	59.	+18.6%
K	1.26	3.16	1.18	2.09	
La	21.2	50.0	33.2	23.6	-41.%
Sm	5.86	13.69	8.7	7.37	-18.0%
Eu	1.57	3.58	0.25	1.91	
Lu	0.431	0.913	0.567	0.671	
Hf	4.10	8.51	7.88	5.35	-64.%
LC-1 to LP-F					
9% Plag - 5% Cpx - 2% Mag					
Co	29.0	31.7	9.5	24.9	
Cr	107.0	46.5	0.002	91.9	+49.%
Sc	29.7	29.5	5.6	22.9	
Ba	325.	376.	322.	605.	+38.%
Rb	—	—	—	19.	
K	0.94	1.09	0.92	1.26	+13.4%
La	13.2	15.2	14.2	21.2	+28.%
Sm	4.75	5.40	4.84	5.86	+7.9%
Eu	1.42	1.61	1.02	1.57	
Lu	0.42	0.46	0.42	0.43	
Hf	3.17	3.67	3.62	4.10	+10.5%
LP-F to AM-6					
35% Plag - 10% Cpx - 10% Opx - 2% Mag					
Co	24.9	34.0	0.06	6.9	
Cr	91.9	13.6	0.002	—	
Sc	22.9	27.9	0.10	16.6	
Ba	605.	1325.	610.	874.	
Rb	19.	43.	32.	45.	+4.4%
K	1.26	2.81	1.19	1.88	
La	21.2	44.7	32.3	22.1	-46.%
Sm	5.86	12.27	8.29	7.17	-15.6%
Eu	1.57	3.21	0.31	1.86	
Lu	0.431	0.829	0.549	0.584	
Hf	4.10	7.75	7.24	4.82	-50.%

Table 6b. Trace Element Results Using Crystal Fractionation Processes.

TRACE ELEMENT	CONC. INITIAL MAGMA	CONCENTRATION PREDICTED HIGH	CONCENTRATION PREDICTED LOW	CONC. FINAL MAGMA	% FROM PREDICTED CONC.
LP-F to AM-2					
40% Plag - 11% Cpx - 11% Opx - 2% Mag					
Co	24.9	37.1	<0.001	4.08	
Cr	91.9	9.4	<0.001	—	
Sc	22.9	29.8	0.03	14.38	
Ba	605.	1592.	604.	953.	
Rb	19.	51.	36.	--	
K	1.26	3.39	1.16	2.13	
La	71.2	53.3	34.3	23.9	-44.%
Sm	5.86	14.61	9.02	8.00	-12.8%
Eu	1.57	3.81	<0.001	1.82	
Lu	0.431	0.971	0.584	0.695	
Hf	4.10	6.91	6.33	5.83	-8.6%
AM-6 to FP-Avg					
26% Plag - 2% Cpx - 6% Opx - 2% Mag					
Co	8.90	10.81	0.20	0.76	
Cr	—	—	—	2.5	
Sc	16.61	22.87	5.48	9.21	
Ba	874.	1271.	837.	950.	
Rb	45.	66.	58.	71.	+7.0%
K	1.88	2.76	1.72	2.52	
La	22.1	31.6	26.8	27.5	
Sm	7.17	10.39	9.28	7.61	-22.%
Eu	1.86	2.67	0.76	1.52	
Lu	0.584	0.833	0.718	0.789	
Hf	4.82	6.54	6.29	8.41	+22.%
AM-Avg to FP-Avg					
16% Plag - 1% Cpx - 2% Opx - 3% Mag					
Co	6.5	7.5	1.9	0.8	-138.%
Cr	4.8	6.5	0.3	2.5	
Sc	15.12	17.59	10.24	9.21	-11.2%
Ba	920.	1129.	876.	950.	
Rb	59.	73.	67.	71.	
K	2.09	2.58	1.93	2.52	
La	23.6	28.7	26.3	27.5	
Sm	7.37	9.05	8.57	7.61	-12.6%
Eu	1.91	2.33	1.08	1.52	
Lu	0.67	0.82	0.76	0.79	
Hf	5.35	6.43	6.28	8.41	+24.%
AM-2 to FP-Avg					
15% Plag - 1% Cpx - 2% Opx - 2% Mag					
Co	4.08	4.66	1.23	0.76	-62.%
Cr	—	—	—	2.5	
Sc	14.38	16.52	9.70	9.21	-5.3%
Ba	953.	1154.	912.	950.	
Rb	—	—	—	71.	
K	2.13	2.59	1.99	2.52	
La	23.9	28.7	26.4	27.5	
Sm	8.00	9.69	9.20	7.61	-21.%
Eu	1.82	2.19	1.08	1.52	
Lu	0.695	0.836	0.782	0.789	
Hf	5.83	6.92	6.77	8.41	+17.7%

TRACE ELEMENT	CONC. INITIAL MAGMA	CONCENTRATION PREDICTED HIGH	CONCENTRATION PREDICTED LOW	CONC. FINAL MAGMA	% FROM PREDICTED CONC.
AM-6 to BOF					
29% Plag - 3% Cpx - 3% Opx - 4% Mag					
Co	8.90	12.04	0.80	0.87	
Cr	--	--	--	--	
Sc	16.61	22.00	4.96	6.36	
Ba	874.	1336.	792.	975.	
Rb	45.	70.	59.	113.	+38.%
K	1.88	2.91	1.61	3.42	+14.9%
La	28.1	33.1	27.5	31.3	
Sm	7.17	10.90	9.53	6.65	-43.%
Eu	1.86	2.79	0.58	0.92	
Lu	0.584	0.869	0.743	0.761	
Hf	4.82	7.11	6.78	8.98	+20.8%
AM-Avg To BOF					
29% Plag - 2% Cpx - 4% Opx - 1% Mag					
Co	6.5	8.6	0.44	0.87	
Cr	4.8	4.6	0.007	—	
Sc	15.12	20.33	4.75	6.36	
Ba	920.	1393.	838.	975.	
Rb	59.	91.	77.	113.	+19.5%
K	2.09	3.20	1.80	3.42	+6.4%
La	23.6	35.1	29.3	31.3	
Sm	7.37	11.1	9.94	6.65	-50.%
Eu	1.91	2.85	0.61	0.92	
Lu	0.671	1.000	0.863	0.761	-13.1%
Hf	5.35	7.73	7.38	8.98	+13.9%
AM-2 to BOF					
29% Plag - 3% Cpx - 3% Opx - 3% Mag					
Co	4.08	5.50	0.37	0.87	
Cr	—	—	—	—	
Sc	14.38	19.00	4.33	6.36	
Ba	953.	1452.	864.	975.	
Rb	—	—	—	—	
K	2.13	3.28	1.83	3.42	+4.1%
La	23.9	35.7	29.7	31.3	
Sm	8.00	12.12	10.61	6.65	-59.%
Eu	1.82	2.72	0.57	0.92	
Lu	0.695	1.032	0.882	0.761	-15.8%
Hf	5.83	8.57	8.17	8.98	+4.6%
AM-6 to CB-3					
31% Plag - 3% Cpx - 4% Opx - 4% Mag					
Co	8.90	12.24	0.42	0.81	
Cr	—	—	—	—	
Sc	16.61	22.95	4.45	9.91	
Ba	874.	1400.	741.	1052.	
Rb	45.	73.	60.	105.	+31.%
K	1.88	3.05	1.60	3.15	+3.2%
La	22.1	34.3	28.2	30.2	
Sm	7.17	11.43	9.87	8.55	-15.4%
Eu	1.86	2.92	0.52	1.27	
Lu	0.584	0.911	0.783	0.901	
Hf	4.82	7.38	6.98	8.02	+7.5%

Table 6c. Trace Element Results Using Crystal Fractionation Processes.

TRACE ELEMENT	CONC. INITIAL MAGMA	CONCENTRATION PREDICTED HIGH	CONCENTRATION PREDICTED LOW	CONC. FINAL MAGMA	% FROM PREDICTED CONC.
AM-Avg to CH-3					
31% Plag - 2% Cpx - 5% Opx - 1% Mag					
Co	6.5	8.8	0.24	0.81	
Cr	4.8	4.75	0.004	--	
Sc	15.12	20.93	5.67	9.91	
Ba	920.	1458.	838.	1052.	+9.5%
Rb	59.	95.	78.	105.	
K	2.09	3.36	1.79	3.15	
La	2.36	36.7	30.0	30.2	
Sm	7.37	11.67	10.30	8.55	-20.5%
Eu	1.91	2.98	0.57	1.27	
Lu	0.671	1.046	0.887	0.901	
Hf	5.35	7.99	7.59	8.02	+0.4%
AM-2 to CH-3					
29% Plag - 2% Cpx - 1% Opx - 3% Mag					
Co	4.08	5.63	1.74	0.81	-1.2%
Cr	--	--	--	--	
Sc	14.38	19.44	7.94	9.91	
Ba	953.	1387.	839.	1052.	
Rb	--	--	--	--	
K	2.13	3.14	1.77	3.15	+0.3%
La	23.9	34.2	29.11	30.2	
Sm	8.00	11.64	10.54	8.55	-23.%
Eu	1.82	2.62	0.58	1.27	
Lu	0.695	0.999	0.887	0.901	
Hf	5.83	8.41	8.02	8.02	
AM-6 to EAB-1					
40% Plag - 3% Cpx - 3% Opx - 4% Mag					
Co	8.90	14.30	0.64	0.37	-73.%
Cr	--	--	--	1.3	
Sc	16.61	26.24	5.00	4.47	-11.9%
Ba	874.	1606.	734.	1090.	
Rb	45.	85.	65.	120.	+29.%
K	1.88	3.52	1.45	3.38	
La	22.1	39.5	30.4	27.0	-9.6%
Sm	7.17	13.15	11.11	5.12	-113.%
Eu	1.86	1.35	0.32	0.83	
Lu	0.584	1.048	0.853	0.451	-89.%
Hf	4.82	8.54	7.94	6.01	-32.%

TRACE ELEMENT	CONC. INITIAL MAGMA	CONCENTRATION PREDICTED HIGH	CONCENTRATION PREDICTED LOW	CONC FINAL MAGMA	% FROM PREDICTED CONC.
AM-Avg to EAB-1					
35% Plag - 4% Cpx - 1% Opx - 4% Mag					
Co	6.5	9.86	1.41	0.37	-281.%
Cr	4.8	3.05	0.09	1.3	
Sc	15.12	21.46	3.68	4.47	
Ba	920.	1521.	790.	1090.	
Rb	59.	100.	80.	120.	+16.7%
K	2.09	3.51	1.67	3.38	
La	23.6	38.2	31.2	27.0	-15.6%
Sm	7.37	12.10	10.26	5.21	-97.%
Eu	1.91	3.09	0.47	0.83	
Lu	0.671	1.073	0.896	0.451	-99.%
Hf	5.35	8.75	8.24	6.01	-37.%
AM-2 to EAB-1					
35% Plag - 3% Cpx - 2% Opx - 4% Mag					
Co	4.08	6.11	0.64	0.37	-73.%
Cr	--	--	--	1.3	-7.8%
Sc	14.38	20.87	4.82	4.47	
Ba	953.	1576.	821.	1090.	
Rb	--	--	--	--	
K	2.13	3.51	1.71	3.38	
La	23.9	38.7	31.9	27.0	-18.1%
Sm	8.00	13.19	11.19	5.21	-118.%
Eu	1.82	3.01	0.42	0.83	
Lu	0.695	1.123	0.945	0.451	-110.%
Hf	5.83	9.42	8.87	6.1	-46.%

basalt-andesite transitions. Barium fits in well in all rhyolite transitions.

Rubidium behaves erratically for the basalt-andesite transitions but generally is not bad considering the low concentrations. For the rhyolites, the actual concentration is above the calculated values. Possible reasons for this include that crystallizing models did not proceed far enough, that the element was concentrated by volatiles, or that the magma was contaminated by the Earth's crust.

Potassium, although not a trace element, generally behaves well for all transitions, but where it does not fit the model, it is higher than the calculated concentrations. Since rubidium and potassium are closely related chemically, they would be expected to behave in similar fashions.

The rare earths behave well in all transitions except for that generating the high silica rhyolite, EAB-1. Europium observed concentrations are bracketed in all cases and deviations for the other rare earth elements may be due to small amounts of apatite which was not considered in the crystal mixing models.

Hafnium behaves rather erratically, sometimes having a higher observed concentration than calculated and sometimes a lower concentration. It is difficult to draw any conclusions in this case.

Conclusions

There are few transitions that appear to be acceptable on the basis of the models used here because, in general, the differences between the calculated concentrations and the observed concentrations are too great for some elements in most transitions. The notable exception is the transition Pri-Mag to B10-1. In most of the other transitions, only one or two observed elemental concentrations vary drastically from the calculated concentrations, but enough to indicate that the model is not a completely satisfactory answer to the problem of magmatic differentiation at Newberry Crater.

The tests of fractional crystallization do not indicate that this is the major method of magma differentiation taking place at Newberry Crater, a conclusion which is consistent with the lack of intermediate silicic rocks. However, fractional crystallization can not be ruled out completely as a means of magma differentiation there. It is probably limited to generating small deviations from the primary magma(s) which may be involved in forming the rocks at Newberry Crater.

SOME ASPECTS OF PARTIAL MELTING

In some ways, partial melting may be thought of as the opposite of fractional crystallization, but there are several important differences. First, a different type of equilibrium is probably involved. The process is most likely a relatively slow one and bulk equilibrium, rather than the surface equilibrium of rapid crystal fractionation, must play the major part as far as laws governing the distribution of minor and trace elements. That in itself is not a problem because this type of equilibrium can be handled theoretically, but the mineral assemblage in the part of the Earth where the partial melting takes place is unknown. Pressure-temperature experiments have been run on several types of rocks, but no definite assemblages have been assigned or even agreed on by petrologists. Green and Ringwood (1968) and O'Hara (1970) attempt to determine the composition of the upper mantle experimentally, but give no indication of what could be called definite assemblages. For this reason, no in-depth attempt will be made to model partial melting as a differentiation process.

Pichler and Kussmaul (1972), Pichler and Zeil (1971), Taylor, et al. (1969), and Kay, et al. (1970) have each proposed partial melting of the crust and upper mantle in various ways to account for the origins and differentiation

of various basalts, andesites, and rhyolites.

Kushiro (1969) and Yoder (1971) have studied partial melting in terms of the diopside-forsterite-quartz system and have advanced the partial melting theory on the basis of high pressure work. The stability fields of the components change vastly between one atmosphere and 20 kilobars of water pressure. The first high silica melt at 20 kilobars pressure lies within the pyroxene stability field of this system. Figure 7 shows the diopside-forsterite-quartz system at one atmosphere pressure with dotted lines and the system at 20 kilobars water pressure with dashed lines. Groupings of the normative analyses of Newberry rocks are also plotted on it.

Yoder (1969) cites experimental evidence for partial melting of a peridotite under different water pressures yielding different mineral assemblages. In dry conditions basaltic rocks (similar to group 1 in Figure 7) are the first formed, in wet conditions at 20 kilobars water pressure rhyolites (similar to group 4 in Figure 7) are first formed and, after the first phase of melting is completed and with an increase of temperature, andesites (similar to the center of group 2 in Figure 7) are the next formed rocks. Points on the normative plot of Newberry rocks, with the exception of the older Amota Butte series, are located near the compositions indicated by Yoder.

Progressive melting with removal of the resulting liquids may be a good type of model to form magmas without

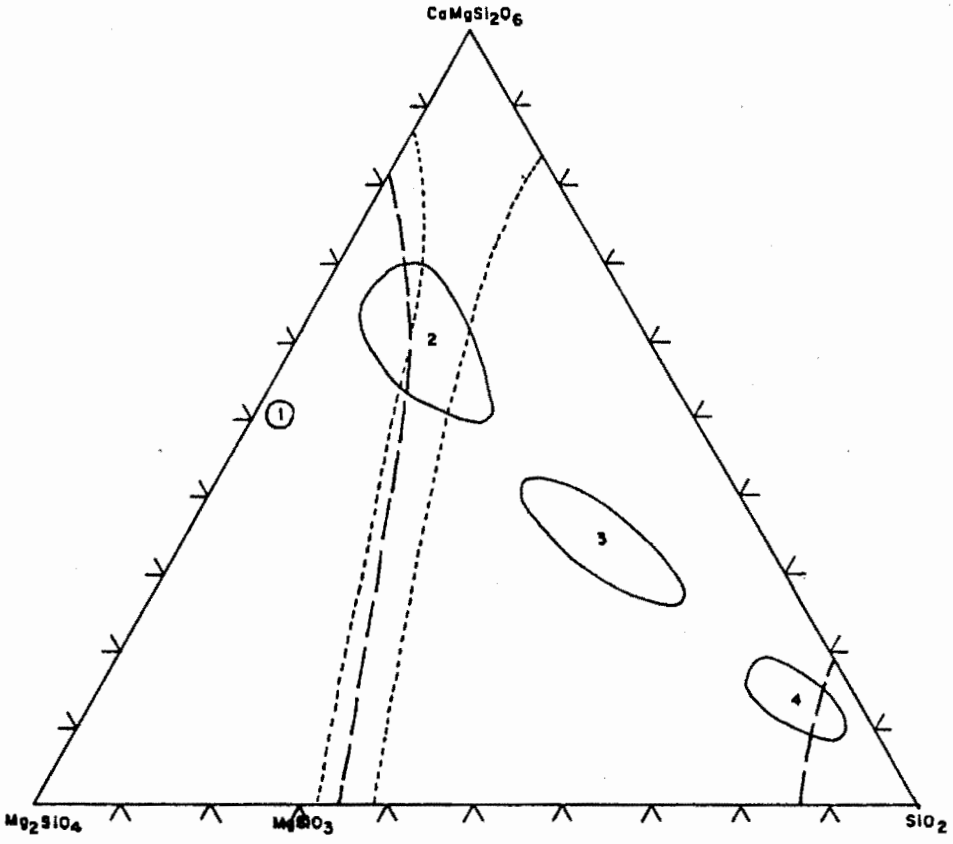

Figure 7. The Diopside-Fosterite-Silica System. The dotted lines indicate fields of stability at 1 atm after Bowen (1928). The dashed lines indicate fields of stability at 20 kb water pressure after Kushiro (1969). The closed lines represent areas corresponding to Newberry samples: 1) FS-B; 2) Basalt-Andesites; 3) Amota Butte Series; and 4) Rhyolites.

having large amounts of intermediate compositions involved. Magmas formed in this manner could be responsible for the primary differences in composition in rocks found at Newberry Crater.

SUMMARY AND CONCLUSIONS

The analytical data for a suite of Newberry Crater rocks are presented in Tables 1a through 1f. Variation diagrams for each element analyzed are given in Figures 3a through 3d.

Four major groupings of rocks are found at Newberry Crater, the basaltic-andesites, the high-iron basalts, the Amota Butte series, and the rhyolites.

The high-iron basalts do not fit well into any scheme or model of differentiation discussed in this dissertation. These rocks are pre-pumice in age, indicating they are pre-collapse in age.

The Amota Butte series of rocks is important in that it may compositionally represent a body of magma apparently involved in a mixing process. The rocks are several miles from the caldera and pre-Mazama ash in age. The fractional crystallization model indicates that their composition can be formed from the basalt-andesite group of rocks except for some trace element abundances.

Examination of the variation diagrams indicates that mixing of two primary magma types may be the main type of magma differentiation process which formed the basaltic-andesite rocks in the suite. The exact silica concentrations of the magmas involved could not be established, but one

must have a silica concentration of around 65% as determined from the chromium variation diagram.

The lack of differentiates with intermediate silica contents and the unsatisfactory results from mixing models argue strongly against fractional crystallization on a large scale as the major means of magma differentiation at Newberry Crater. It may account for deviations from the mixing line and other small observed differences in the rocks.

The pumice, cinder cones, and vesicles in lava indicate that volatile transfer might have played a minor part at Newberry Crater.

As exemplified by Yoder's work with the diopside-forsterite-silica ternary diagram, partial melting may help explain the composition of rocks at Newberry Crater. With our present knowledge, this does not explain the composition of the Amota Butte series nor the linear trend of compositions of the basaltic-andesites toward the Amota Butte series. No single model is likely to explain magma differentiation and rock relationships at Newberry Crater.

APPENDIX I

SAMPLE LOCATIONS

Appendix I gives the locations from which samples were collected and contains topographical maps of the Newberry Crater Quadrangle for reference. The order of samples corresponds to that in Tables 1a through 1f.

Basalt-Andesites

SP-1 Sugar Pine Butte Flow R11E, T20S, Sec 23. Northwest slope from beside road.

RS Red Slide Cinder Cone R12E, T21S, Sec 23. Wall of crater north of Paulina Lake.

SSP-F South Sugar Pine Flow R11E, T20S, Sec 25. Northwest slope from dead end road at base of unnamed butte.

B8-5 Kwinnum Butte Flow R12E, T20S, Sec 35. Pre-Mazama flow from roadcut.

FU-B Fuzztail Butte Cinder Cone R13E, T20S, Sec 6. Northeast slope.

PI-B Pilpil Butte Cinder Cone R12E, T21S, Sec 1. North slope, upper of two flows in roadcut.

LR-1 Lava Road Flow R12E, T20S, Sec 21. Northwest fissure near road.

DG-2 Unnamed Dry Gulch Flow R11E, T21S, Sec 11. Northwest slope, upper of two flows in roadcut.

LCF-F Lava Cast Forest Flow R12E, T20S, Sec 34. Northwest fissure south of campground.

RE-B Red Butte Cinder Cone R13E, T23S, Sec 22. Southeast slope.

ILB Interlake Basalt Flow R12E, T21S, Sec 25. Crater floor from north wall, sample from above trail on Paulina Lake shore.

PPCC-1 North Paulina Peak Cinder Cone R12E, T21S, Sec 24. North slope near crater.

DH-B Devils Horn Butte Cinder Cone R13E, T22S, Sec 17. Southeast slope.

CH-B Cinder Hill Butte Cinder Cone R13E, T21S, Sec 14. Northeast slope, this sample is post-Newberry pumice in age.

CH-F Cinder Hill Flow (not from Cinder Butte) R13E, T21S, Sec 14. This sample is pre-Newberry Pumice from a roadcut 1/4 mile east of Cinder Hill Butte, northeast slope.

NS-1 North Summit Flow R12E, T21S, Sec 13. On northwest fissure.

LC-1 Lava Cascade Flow R12E, T21S, Sec 3. Northwest fissure from lower part of cascade.

LP-F Lava Pass Flow R12E, T20S, Sec 31. Northwest fissure from near road.

SU-F Surveyor Flow R12E, T22S, Sec 32. South slope.

F-1 Fissure Cinder R13E, T21S, Sec 19. North wall of caldera, north of East Lake.

B10-1 Resort Lava Flow R13E, T21S, Sec 29. Caldera floor.

MB-1 Mokst Butte Flow R12E, T20S, Sec 22. Northeast slope.

EPP-2 East Paulina Peak Cinder Cone R13E, T21S, Sec 28. East slope between caldera wall and east fissure.

TV-F Twin Vents Flow R12E, T20S, Sec 22. Northwest fissure.

FI-B Finley Butte Cinder Cone R11E, T22S, Sec 20. Southwest slope.

LB-1 through LB-5 Lava Butte Flows representing five distinct flow units R11E, T19S, Sec 24. Extreme end of northwest fissure.

High-Iron Basalts

DG-1 Unnamed Dry Gulch Flow R11E, T21S, Sec 11. Northwest slope, lower of two flows in road cut.

NPP-1 through NPP-3 North Paulina Peak Flows R12E, T21S, Sec 24. North-central caldera wall.

F-2 Fissure Cinder Cone R13E, T21S, Sec 19. North caldera wall above East Lake.

A2-3 North Wall Andesite Flow R12E, T21S, Sec 24. North caldera wall.

Amota Butte Series

AM-1 through AM-8 Amota Butte Flows R13E, T23S, Sec 28. Southeast slope, from pre-Mazama pumice fault scarp.

Rhyolites

PP-4 through PP-9 South Paulina Peak Rhyolites R12E, T22S, Sec 10, 11. Roadcut samples.

R8-2 Rhyolite Dome R13E, T21S, Sec 31. East of Big Obsidian Flow on caldera flow. floor

PUMICE From beside road near southeast rim of crater.

R8-3 Rhyolite R13E, T21S, Sec 20. Float from north side of East Lake.

BOF Big Obsidian Flow R12E, T21S, Sec 36. Toe of flow. 18

ILO Interlake Obsidian Flow R12E, T21S, Sec 25. Near Paulina Lake. 19

CH-1 and CH-3 China Hat Rhyolite Dome R14E, T22S, Sec 10. East slope from road cuts.

MC-2A and MC-2B McKay Butte Rhyolite Dome R11E, T21S, Sec 24. West slope.

EAB-1 and EAB-3 East Butte Rhyolite Dome R14E, T22S, Sec 13. East slope from road cuts (just off map on Figure I-1d, see Figure 1).

Newberry Area Samples

FS-B Firestone Butte Flow R15E, T22S, Sec 7. East slope, pre-Newberry pumice (just off map on Figure I-1d, see Figure 1).

PF-1 Paulina Falls Tuff R12E, T21S, Sec 34. Thick unit below falls.

17, 8, and 19 High Cascade Flows from the McKenzie Pass area (not on maps).

8 Sims Butte on Route 242 from vertical cut.

17 Little Belnap Flow on the Skyline Trail 1 1/2 miles west of Dee Wright Observatory.

19 Yapoah Cone 1 1/2 miles northwest of Black Crater.

BRB-Q Black Rock Butte Flow R7E, T24S, Sec 24. High Cascades quartz bearing basalt (not on maps).

PM-1 and PM-3 Pine Mountain Rhyolite R15E, T20S, Sec 28 and R15E, T21S, Sec 9. 1 from road cut and 3 from bluff 1/4 mile northwest of road (see Figure 1).

PM-2 Pine Mountain Andesite R15E, T20S, Sec 28. From road cut (see Figure 1).

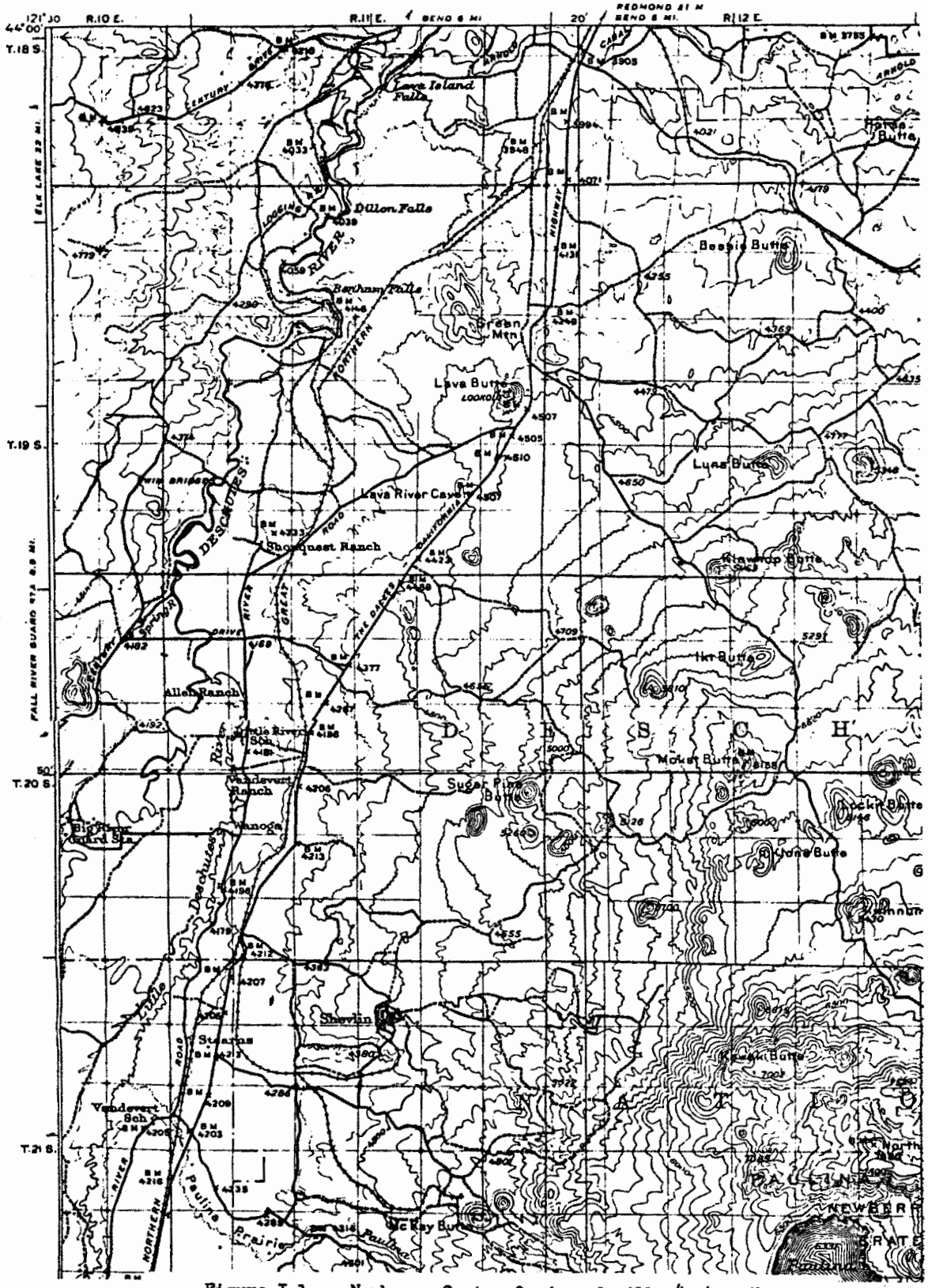

Figure I-1a. Newberry Crater Quadrangle NW 1/4 (1935).

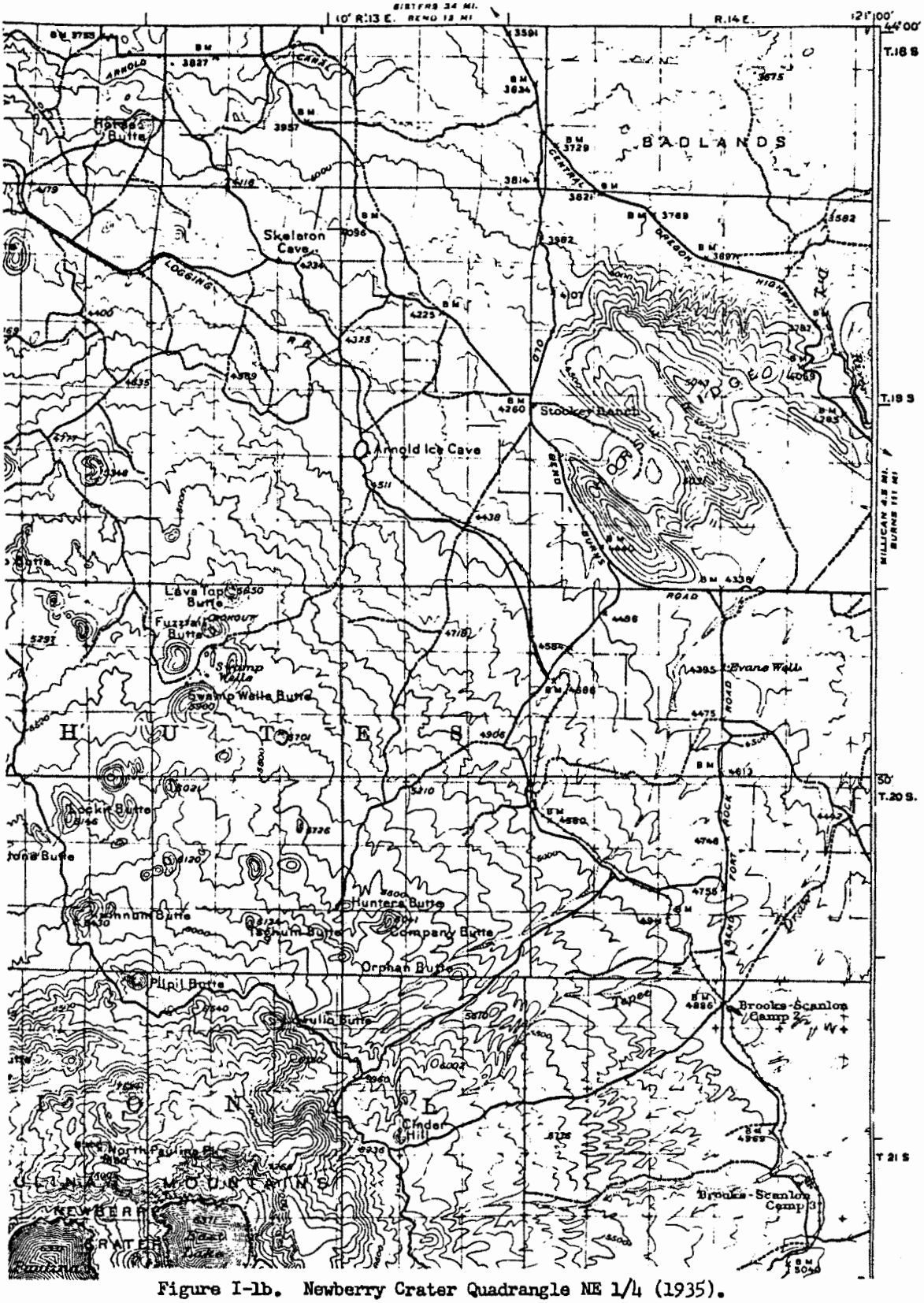

Figure I-1b. Newberry Crater Quadrangle NE 1/4 (1935).

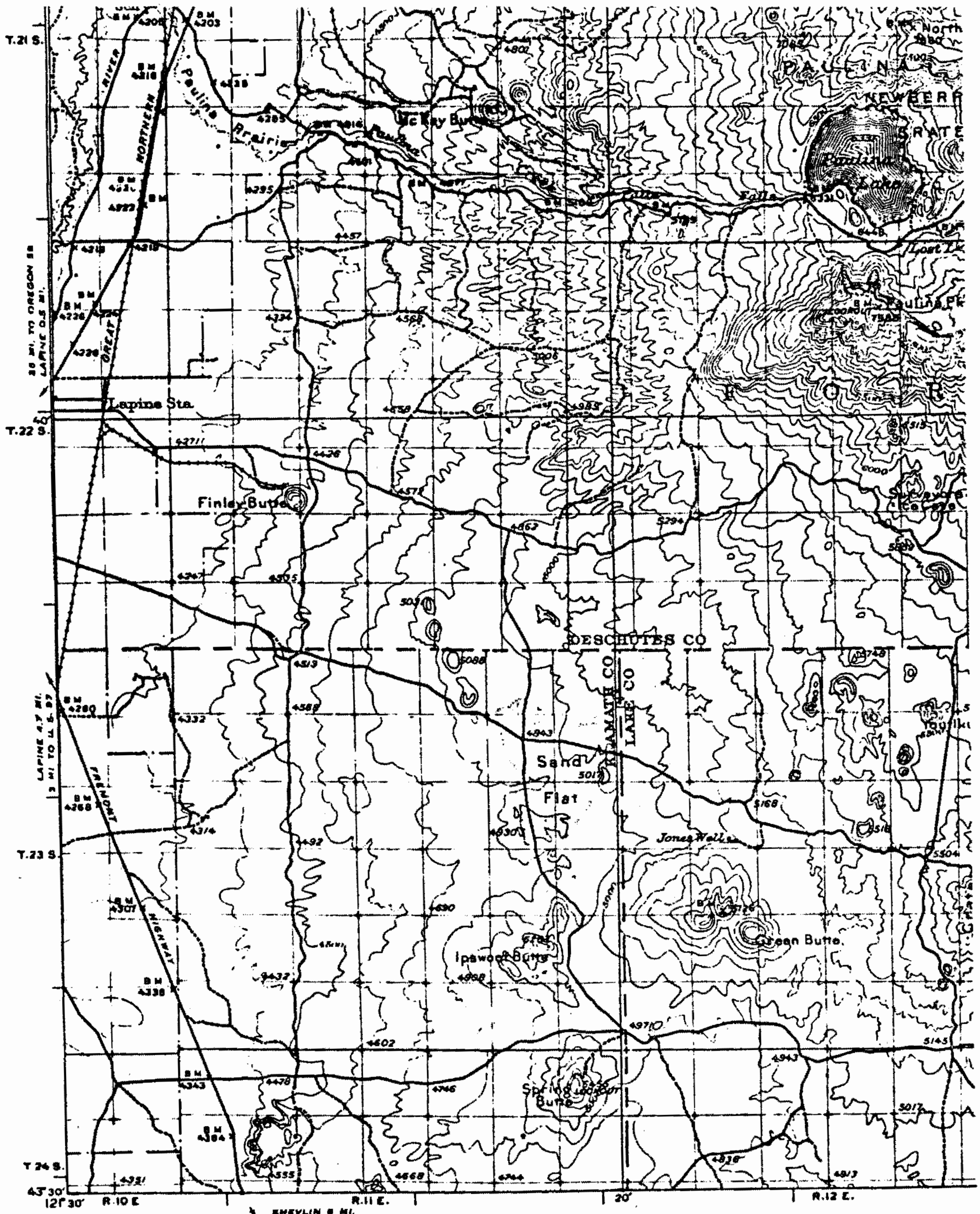

Figure I-1c. Newberry Crater Quadrangle SW 1/4 (1935).

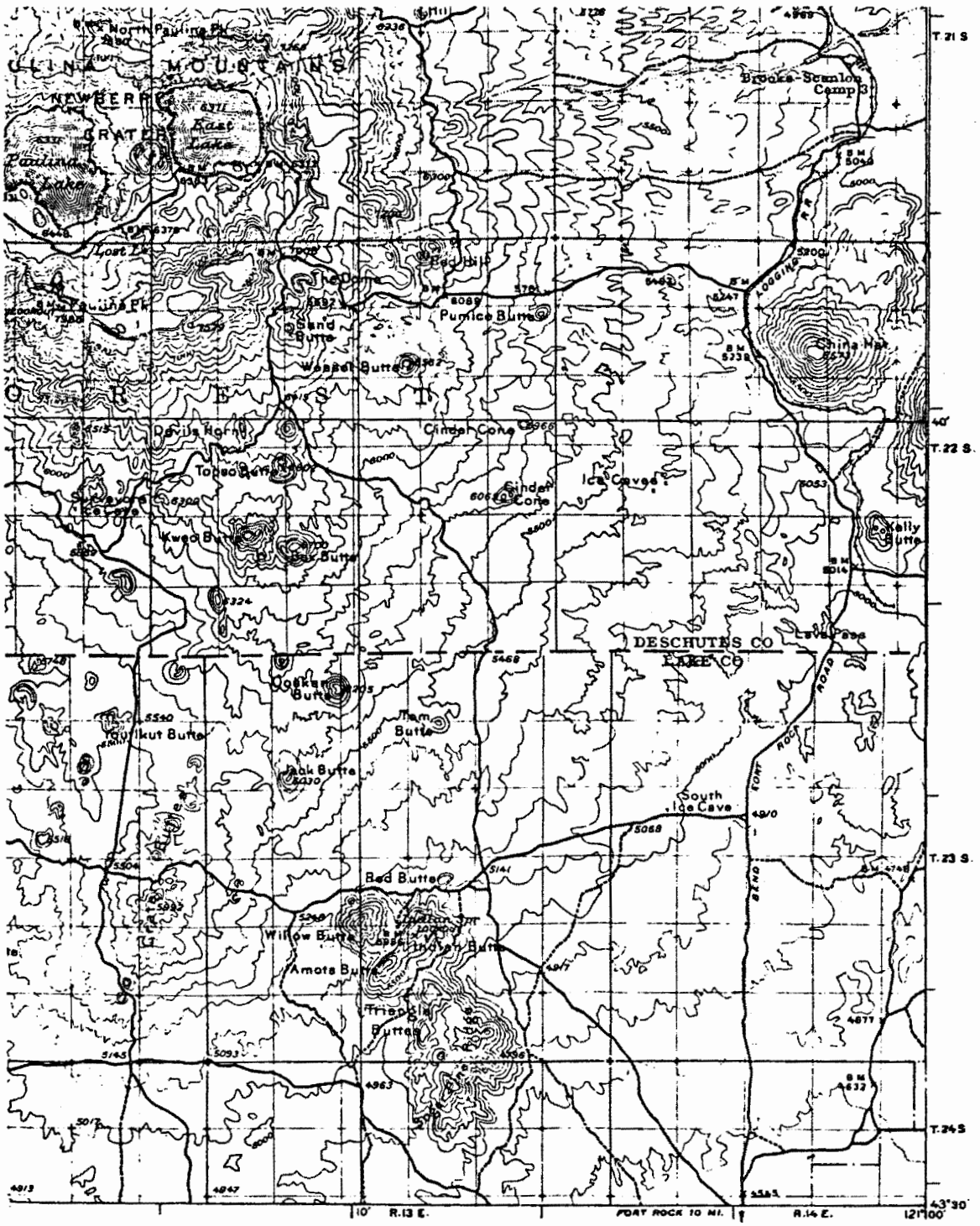

Figure I-1d. Newberry Crater Quadrangle SE 1/4 (1935).

APPENDIX II

MOLECULAR NORM CALCULATIONS

Norms are recalculated rock analyses in which oxide analyses are converted into a standard set of mineral molecules. They offer a system in which rock analyses can be quantitatively studied and compared from a petrological point of view. The calculations are simple and, in most cases, the normative minerals correspond well with minerals observed in natural systems.

Norm calculations must be made in the right sequence and the rules for the calculations adapted from Barth (1951) follow. These rules are based on equivalent molecular units for ease in calculations.

1. Calcite is formed from CO_2 and an equal amount of CaO.

2. Apatite, AP, is formed from P_2O_5 and 3.33 times this amount of CaO.

3. Pyrite is formed from S and half this amount of FeO.

4. Ilmenite, IL, is formed from TiO_2 and an equal amount of FeO.

5. The alkali feldspars (orthoclase, OR, and albite, AB) are formed provisionally from K_2O and Na_2O combined in

the right proportions with Al_2O_3 and SiO_2.

6a. If there is an excess of Al_2O_3 over $K_2O + Na_2O$, it is assigned to anorthite, AN, one half the remaining amount of CaO being allotted to the excess of Al_2O_3.

6b. If there is an excess of Al_2O_3 over this CaO, it is calculated as corundum, CO.

6c. If there is an excess of CaO over this Al_2O_3 of 6a, it is reserved for wollanstonite, WO (8).

7a. If in 5 there is an excess of Na_2O over Al_2O_3, it is to be combined with an equal amount of Fe_2O_3 to form the acmite molecule. There is then no anorthite in the norm.

7b. If, as usually happens, there is an excess of Fe_2O_3 over Na_2O, it is assigned to magnetite, MT, one half the remaining amount of FeO being allotted to it out of what remains from the formation of pyrite and ilmenite.

8. Wollanstonite, WO, is formed from the amount of CaO left over from 6a.

9. Enstatite, EN, and ferrosilite, FS, are formed provisionally from all the MgO and FeO remaining from the previous allotments.

10a. If there is an excess of SiO_2, it is calculated as quartz, QZ.

10b. If there is a deficiency of SiO_2, minerals of a lower degree of silification have to substitute, in part or wholly, for those minerals that were formed provisionally. Wollanstonite, WO, would be combined with an equal amount of

enstatite, EN, plus ferrosilite, FS, to form diopside, DI. The excess enstatite and ferrosilite form hypersthene, HY. The proportion of FeO to MgO should be the same for diopside, hypersthene, and olivine.

10c. The necessary amount of enstatite and ferrosilite remaining from 10b is converted into olivine, OL (forsterite, FO, and fayalite, FA), according to the equation

$$4EN = 3FO + 1QZ.$$

10d. If there still is not enough SiO_2 in the analysis, albite, AB, is turned into nepheline according to the equation

$$5AB = 3NE + 2QZ.$$

10e. Finally, if the analysis is very low in SiO_2 orthoclase, OR, is in part or wholly converted into leucite

$$5OR = 4LE + 1QZ.$$

10f. In rare cases there is not even enough SiO_2 to form leucite. Then kaliophilite is formed

$$4LE = 3KP + 1QZ.$$

BIBLIOGRAPHY

Barth T. F. W. (1951) Theoretical Petrology. John Wiley and Sons, Inc., New York.

Bowen N. L. (1928) The Evolution of the Igneous Rocks. Dover Publications, Inc., New York.

Bryan W. B., Finger L. W., and Chayes F. (1969) Estimating proportions in petrographic mixing equations by least squares approximations. Science 163, 926-927.

Corliss J. B. (1970) Mid Ocean Ridge Basalts: I - The origin of submarine hydrothermal solutions; II - Regional diversity along the mid-Atlantic ridge. Unpublished Ph.D. dissertation, University of California, San Diego.

Drake M. J. (1972) The Distribution of Major and Trace Elements Between Plagioclase Feldspar and Magmatic Silicate Liquid: An Experimental Study. Unpublished Ph.D. dissertation, University of Oregon, Eugene.

Dudas M. J., Schmitt R. A., and Harward M. E. (1971) Trace element partitioning between volcanic plagioclase and dacitic pyroclastic matrix. Earth Planet. Sci. Let. 11, 440-446.

Ewart A. and Taylor S. R. (1969) Trace element geochemistry of the rhyolitic volcanic rocks, central North Island, New Zealand. Phenocryst data. Contr. Mineral. and Petrol. 22, 127-146.

Gordon G. E., Randle K., Goles G. G., Corliss J. B., Beeson M. H., and Oxley S. S. (1968) Instrumental activation analysis of standard rocks with high-resolution X-ray detectors. Geochim. Cosmochim. Acta 32, 369-396.

Green T. H. and Ringwood A. E. (1968) Genesis of the calc-alkaline igneous rock suite. Contr. Mineral. and Petrol. 18, 105-162.

Higgins M. W. (1973) Petrology of Newberry Volcano, Central Oregon. Geol. Soc. America Bull. 84, 455-488.

Higgins M. W. and Waters A. C. (1967) Newberry caldera, Oregon: A preliminary report. The Ore Bin 29, 37-60.

Higgins M. W. and Waters A. C. (1968) Newberry caldera field trip, Andesite Conference Guide Book - State of Oregon, Department of Geology and Mineral Industries. Bulletin 62, 59-77.

Higgins M. W. and Waters A. C. (1970) A re-evaluation of basalt-obsidian relations at East Lake fissure, Newberry caldera, Oregon. Geol. Soc. America Bull. 81, 2835-2842.

Hiquchi H. and Nagasawa H. (1969) Partition of trace elements between rock-forming minerals and the host volcanic rocks. Earth Planet. Sci. Let. 7, 281-287.

Kay R., Hubbard N. J., and Gast P. W. (1970) Chemical characteristics and origin of oceanic ridge volcanic rocks. Jour. Geophys. Res. 75, 1585-1613.

Kushiro I. (1969) The system forsterite-diopside-silica with and without water at high pressures. Am. Jour. Sci. 267-A (Schairer Volume), 269-294.

Laidley R. A. and McKay D. S. (1971) Geochemical examination of obsidians from Newberry caldera, Oregon. Contr. Mineral. and Petrol. 30, 336-342.

Libby W. F. (1952) Chicago radiocarbon dates, III. Science 116, 673-681.

Lorenz V. (1970) Some aspects of the eruption mechanism of the Big-Hole marr, Central Oregon. Geol. Soc. America Bull. 81, 1823-1829.

Mason B. (1966) Principles of Geochemistry. John Wiley and Sons, Inc., New York.

Norrish K. and Hutton J. T. (1969) An accurate X-ray spectrographic method for the analysis of a wide range of geological samples. Geochim. Cosmochim. Acta 33, 431-453.

Osborn T. W. and Schmitt R. A. (1970) Sodium and manganese homogeneity in chondritic meteorites. Icarus 13, 207-214.

O'Hara M. J. (1970) Upper mantle composition inferred from laboratory experiments and observation of volcanic products. Phys. Earth Planet. Interiors 3, 236-245.

Peterson N. V. and Groh E. A. (1965) Lunar Geological Field Conference Guide Book - State of Oregon Department of Geology and Mineral Industries Bulletin 57.

Peterson N. V. and Groh E. A. (1969) The ages of some Holocene volcanic eruptions in the Newberry Volcano area, Oregon. The Ore Bin 31, 73-87.

Philpotts J. A. and Schnetzler C. C. (1970) Phenocrysts matrix partition coefficients for K, Rb, Sr, and Ba, with applications to anorthosite and basalt genesis. Geochim. Cosmochim. Acta 34, 307-322.

Pichler H. and Kussmaul S. (1972) The calc-alkaline volcanic rocks of the Santorini Group (Agean Sea, Greece). Neues Jahrbuch für Mineralogie Abh. 116, 268-307.

Pichler H. and Zeil W. (1971) The cenozoic rhyolite-andesite association of the Chilean Andes. Bull. Volcanologique 35, 424-452.

Robinson P. T. (1969) High-titania alkali-olivine basalts of North-Central Oregon, U. S. A. Contr. Mineral. and Petrol. 22, 349-360.

Roedder E. and Weiblen P. W. (1971) Petrology of silica melt inclusions, Apollo 11 and Apollo 12 and terrestrial equivalents. in Proceedings of the Second Lunar Science Conference, Vol. 1 (A. A. Levinson, Ed.), 507-528, The M. I. T. Press, Cambridge.

Schnetzler C. C. and Philpotts J. A. (1968) Partition coefficients of rare earth elements and barium between igneous matrix material and rock-forming mineral phenocrysts. I. in Origin and Distribution of the Elements (L. H. Ahrens, Ed.), 929-938, Pergamon Press, Oxford.

Schnetzler C. C. and Philpotts J. A. (1970) Partition coefficients of rare earth elements between igneous matrix material and rock-forming mineral phenocrysts, II. Geochim. Cosmochim. Acta 34, 331-340.

Stonesifer C. A., Courtney R. D., and Fischer G. A. (1931) Newberry Crater Quadrangle, Oregon. United States Department of Interior Geological Survey.

Taylor S. R. (1966) The application of trace element data to problems in petrology. in Physics and Chemistry of the Earth (L. H. Ahrens, F. Press, and S. K. Runcorn, editors), 133-213, Pergamon Press, Oxford.

Taylor S. R., Kay M., White A. J. R., Duncan A. R., and Ewart A. (1969) Genetic significance of Co, Cr, Ni, Sc, and V content of andesites. Geochim. Cosmochim. Acta 33, 275-286.

Turner F. J. and Verhoogen J. (1951) Igneous and Metamorphic Petrology. McGraw Hill, New York.

United States Department of Agriculture, Deschutes National Forest. The Lava Butte Geological Area. Story by P. G. Brogan.

United States Department of Agriculture, Deschutes National Forest. The Newberry Crater of Central Oregon.

Waters A. C. (1961) Stratigraphic and lithologic variations in the Columbia River basalt. Am. Jour. Sci. 259, 583-611.

Williams H. (1935) Newberry volcano of Central Oregon. Bull. Geol. Soc. Am. 46, 253-304.

Williams H. (1957) A Geological Map of the Bend Quadrangle, Oregon, and a Reconnaissance Geologic Map of the Central Portions of the High Cascade Mountains. State of Oregon Department of Geology and Mineral Industries.

Williams H., Turner F. J., and Gilbert C. M. (1954) Petrography - An Introduction to the Study of Rocks in Thin-Sections. W. H. Freeman and Co., San Francisco.

Yoder H. S. (1969) Calcalkalic andesites: Experimental data bearing on the origin of their assumed characteristics, Proceedings of the Andesite Conference - State of Oregon, Department of Geology and Mineral Industries. Bulletin 65, 77-89.

Yoder H. S. (1971) Contemporaneous rhyolite and basalt. Carnegie Institution Washington Year Book 69, 141-145.

Yoder H. S. (1973) Contemporaneous basaltic and rhyolitic magmas. Am. Mineralogist 58, 153-171.